THE ASTROPHYSICAL JOURNAL SUPPLEMENT SERIES, 61:531–568, 1986 July

CHROMOSPHERIC ACTIVITY, KINEMATICS, AND METALLICITIES OF NEARBY M DWARFS[1]

JOHN R. STAUFFER[2]
Dominion Astrophysical Observatory, Herzberg Institute of Astrophysics
AND
LEE W. HARTMANN
Harvard-Smithsonian Center for Astrophysics
Received 1985 September 30; accepted 1985 December 18

ABSTRACT

A summary of more than 1000 observations of approximately 200 Gliese catalog M dwarfs is presented. The *BVRIJHK* photometry is believed to be accurate to 0.015 mag in each passband. Radial velocities accurate to 1 km s^{-1}, Hα equivalent widths accurate to 0.03 Å, and Gaussian widths for the Hα profile accurate to 10% have been derived from echelle spectra. Rotational velocity estimates derived from cross-correlation analysis are provided for a few stars. Low-dispersion spectra have been used to calibrate a relation between TiO band strength and $(R-I)$ color, and to compare the surface gravities of subdwarfs and normal dM stars.

Our analysis of these new data show that the Hα equivalent widths are a useful chromospheric indicator for M dwarfs. The oldest, and presumably least chromospherically active, M dwarfs in our sample generally have weak Hα absorption lines. As the chromosphere increases in strength, the Hα absorption equivalent width first increases, then decreases again, and finally Hα goes into emission. This is the behavior predicted by Cram and Mullan for M dwarf chromospheres. Assuming that the decrease in chromospheric activity with time can be modeled adequately as an exponential, a very rough estimate yields approximately 10^9 years as the *e*-folding time scale. We provide a list of all the dMe stars in our sample, as well as another list of stars with only slightly less active chromospheres based on the apparent filling in of their Hα absorption profile.

We have used our *JHK* photometry to identify stars with metallicities significantly different from that of the Sun. The M dwarfs with approximately solar metallicity have been used to define a zero-age main sequence locus. The resultant main-sequence relation is $M_V = 5.31(R-I)_K + 5.24$, valid between $R-I=0.65$ and $R-I=1.10$. This agrees quite well with a main-sequence locus derived from a fit to Hyades and Praesepe M dwarfs, if $(m-M)_0 = 3.30$ is assumed for the Hyades and if a metallicity correction appropriate to [M/H] = +0.15 is applied to the cluster stars.

The dMe stars in our sample generally have young disk motions, are more luminous than dM stars of the same color, and have $B-V$ colors too blue for their $V-I$ color. A small subset of the dMe stars, however, have old disk motions, are displaced below the main sequence, and are red in $B-V$ for their $V-I$. A range in metallicity among the dMe stars, with most of them more metal-rich than the Sun, can explain this result. The characteristic that unifies the dMe stars appears to be rotation. Eleven of the 29 dMe stars in our sample have rotational velocities above our detection limit of 10 km s^{-1}, while only one or two of the approximately 170 dM stars may have measurable $v \sin i$ values. Rotational velocity determinations for several of our dMe stars have been previously reported. When all sources of rotational velocity data are considered, more than half of our dMe stars have known or inferred rotational velocities greater than 5 km s^{-1}, in accord with Bopp's hypothesis of a trigger velocity for the dMe phenomenon.

Subject headings: photometry — stars: abundances — stars: chromospheres — stars: rotation — stars: stellar dynamics — stars: variables

I. INTRODUCTION

Considerable effort has been expended over the last 20 years in monitoring the chromospheric activity of solar-type stars via the Ca II H and K lines (Wilson 1966, 1978; Vaughan and Preston 1980). These data have been used primarily to estimate stellar rotational periods (Vaughan *et al.* 1981; Duncan *et al.* 1984; Noyes *et al.* 1984) and as one measure of the amount of nonradiative chromospheric heating in late-type stars with outer convective envelopes (Linsky and Ayres 1978; Vernazza, Avrett, and Loeser 1981). When combined with age estimates for the program stars, the Ca II H and K observations provide empirical constraints for theoretical models of the evolution of magnetic dynamos (Parker 1979; Noyes *et al.* 1984) and angular-momentum loss rates

[1]Research reported here used the Multiple Mirror Telescope Observatory, a joint facility of the Smithsonian Institution and the University of Arizona.

[2]Visiting Astronomer, Kitt Peak National Observatory, which is operated by the Association of Universities for Research in Astronomy, Inc., under contract with the National Science Foundation.

(Durney, Mihalas, and Robinson (1981) for solar-type stars. With the development of red-sensitive, digital detectors, Herbig (1985) has shown that quantitative measures of the Hα equivalent widths in G stars correlate well with the Ca II H and K data, and could be used for similar purposes.

While the literature related to the chromospheric activity of G and K dwarfs is quite extensive, M dwarfs have been, by comparison, sadly neglected. Some Ca II H and K data are available for nearby M dwarfs, but these data have not been extensively analyzed. Because M dwarfs are much brighter at 6500 Å than at 3900 Å, Hα may be a preferable chromospheric diagnostic. The use of Hα equivalent widths as an indicator of chromospheric activity in M dwarfs has been discussed by Giampapa (1985) and Zarro (1983). High-resolution spectroscopic data at Hα for a few dM and dMe stars have been published by Kraft, Preston, and Wolff (1964), Worden, Schneeberger, and Giampapa (1981), and Zarro and Rodgers (1983). A first step toward providing quantitative estimates of the chromospheric activity of a large sample of randomly selected M dwarfs has recently been presented by Young *et al.* (1986, hereafter Paper I). Those authors outlined preliminary results of spectroscopic surveys of the Hα strengths in late K and M dwarfs by Bopp; by Young, Skumanich, and Harlan (1984); and by Stauffer and Hartmann (1985). In this paper we will present a more complete discussion of our spectroscopic survey.

We have also obtained new *BVRIJHK* photometry of a large sample of M dwarfs. A number of other authors have previously conducted photometric surveys of nearby, field M dwarfs (Spinrad 1973; Veeder 1974*a*; Mould and Hyland 1976; Hartwick 1977; Eggen 1979, 1980; Harrington and Dahn 1980; and Weis and Upgren 1982). Those studies have been useful for providing estimates of the bolometric luminosities and effective temperatures for a moderately large sample of stars. A conclusion common to most of the above-cited papers was that there appears to be an unexpectedly large spread in luminosity, at fixed effective temperature, among the M dwarfs. The authors ascribed that spread to a number of possible causes, including age differences (sufficiently young dM stars might still be on their pre–main-sequence evolutionary tracks, and hence be overluminous), metallicity differences (due either to blanketing effects causing color shifts or to real luminosity effects), and insufficient correction for binarity.

In the analysis of our new photometric survey, we have two major advantages relative to the previous efforts. Of primary importance, we have obtained echelle spectra for a large fraction of the stars observed photometrically. This allows us to determine accurate Hα equivalent widths, radial velocities, and in a few cases rotational velocities for those stars. In most cases we have two or more spectra per star, and so we have an indication of radial velocity variability. Hence, we have independent data which give information related to the ages, metallicities, and binarity of the program stars. The second advantage we have is our sample size, which is about 200 stars, double the size of the previous most extensive survey. The large sample size allows us to isolate subsets of stars with particular characteristics to test specific hypotheses, and still have enough stars to obtain meaningful results.

Specifically, we provide here a homogeneous set of new *BVRIJHK* photometry of Gliese (1969*a*) catalog M dwarfs. In Paper I, we have provided a preliminary list of Hα equivalent widths derived from our 0.15 Å resolution echelle spectra. In this paper, we provide a slightly updated set of Hα equivalent widths, as well as the FWHM of the Hα line, and radial velocities accurate to about 1 km s^{-1} derived from cross-correlation routines. Narrow-band line strengths obtained from low-dispersion spectra for a small sample of Gliese catalog stars are also provided.

These data are used to examine more closely the (Hα, $R-I$)-diagram introduced in Paper I. How do metallicity and age affect the location of stars in that diagram? How do the Hα profiles and equivalent widths for real stars compare with the model M dwarfs of Cram and Mullan (1979)? We also examine the influence of metallicity and chromospheric activity on the H-R diagram for low-mass stars. We particularly wish to derive a solar-metallicity, zero-age main sequence (ZAMS) for stars with $M < 0.6\ M_{\odot}$ in order to compare with our open cluster photometry (Stauffer 1982*a*, *b*, 1984; Stauffer, Hartmann, and Jones 1985).

The format of the paper is conventional. Section II is devoted to the presentation of the new observational results. Analysis of the Hα versus $R-I$ diagram is provided in § III. Construction of a solar-metallicity ZAMS is outlined in § IV, along with comparisons of our result with previous calibrations. The final section considers the implications of our data for the origin of dMe stars.

II. OBSERVATIONAL DATA

The primary sample of stars chosen for study included all Gliese catalog M dwarfs with spectral type according to Gliese (1969*a*) later than M0, *V*-magnitude brighter than or equal to 12.0, and north of declination $-10°$. Secondary stars of binary systems where the primary is considerably brighter and the angular separation is less than 30″ were also excluded because of the difficulty of obtaining accurate photometry for those stars. The final list includes 203 stars. Our level of completeness in the observation of that sample is 66%, 87%, and 70% for the *BVRI*, echelle spectroscopy, and infrared photometry surveys, respectively. The stars not observed at *BVRI* are primarily those for which good photometry already exists in the literature; the stars not observed with the echelle are generally in the right ascension range that conflicts with our open cluster program ($3^h < \text{R.A.} < 8^h$); the infrared program lacks data for $22^h < \text{R.A.} < 4^h$. We have also observed another set of Gliese (1969*a*) and Woolley *et al.* (1970) M dwarfs that do not satisfy all of the above criteria. These stars were chosen primarily because of their favorable right ascensions (i.e., there were no more primary program objects in that part of the sky). As a result of these additional observations, the total number of stars for which we have new data is 202 (echelle), 199 (*BVRI*), and 156 (*JHK*). In our analysis, we will treat the entire data set, regardless of whether the star is part of the primary sample, since we are not attempting to derive parameters dependent on the completeness of our sample.

a) *Optical Photometry*

Most of our optical photometry was obtained at Kitt Peak National Observatory using the 1.3 m telescope, the Mk II computer-controlled photometer, and an RCA C31034A phototube. The filters employed were the Kitt Peak "special" *BVRI* filter set. A small number of stars were also observed using similar instrumental systems at the Kitt Peak No. 2 0.9 m and the CTIO 1.5 m telescopes. Reduction to the Johnson B and V, and Kron R and I photometric systems was accomplished through standard stars selected from Kron, Gascoigne, and White (1957, hereafter KGW), Eggen (1975), Moffett and Barnes (1979), and Landolt (1983). For very red stars we have adopted Eggen's $R-I$ standard values (see Stauffer 1982*a*),[3] and thus our $R-I$ system differs slightly from that derived by Weis and Upgren (1982). Nearly all of the M dwarf photometry was obtained during observing runs scheduled for open cluster programs during 1979–1985. The open cluster data have been published elsewhere (Stauffer 1980, 1982*a*, *b*, 1984; Stauffer, Hartmann, and Jones 1985).

Results of the photometry program are supplied in Table 1. Columns (1)–(6) provide, in order, the Gliese catalog designation, an alternative name for the star, the mean V-magnitude, and $B-V$, $V-R$, and $R-I$ colors for each star.

Estimates of the accuracy of the photometry can be derived in several ways. Integration times were always sufficiently long so that the expected errors solely from photon statistics are less than 1% for V, $V-R$, and $R-I$. The expected error in $B-V$ for most of the program stars was also 1% or less, but for the faintest and reddest stars the error was allowed to rise to 2%. A more realistic estimate of the photometric accuracy obtained can be derived from examination of the stars observed repeatedly. For the 14 stars observed more than four times each (and not used as standards), standard deviations of the magnitudes and colors were calculated. The mean values of those standard deviations are $\langle\sigma(V)\rangle = 0.010$ mag, $\langle\sigma(B-V)\rangle = 0.012$ mag, $\langle\sigma(V-R)\rangle = 0.011$ mag, and $\langle\sigma(R-I)\rangle = 0.008$ mag. The best external check on the accuracy of our (SH) photometry can be obtained by comparison with the published photometry of Eggen (1979,1980). For the approximately 50 stars in common between the two data sets, the means and standard deviations in the sense (SH − Eggen) are

$$\langle(V_{SH}-V_E)\rangle = -0.006, \quad \sigma = 0.039,$$

$$\langle(B-V)_{SH}-(B-V)_E\rangle = -0.004, \quad \sigma = 0.023,$$

$$\langle(V-R)_{SH}-(V-R)_E\rangle = -0.016, \quad \sigma = 0.053,$$

$$\langle(R-I)_{SH}-(R-I)_E\rangle = \quad 0.013, \quad \sigma = 0.022.$$

[3] Two of the stars listed in Table 4 of Stauffer (1982*a*) have incorrectly listed assumed standard magnitudes and colors. The correct values for those stars are the following: for VA 68, $V = 10.70$, $B-V = 1.21$, $V-R = 0.70$, $R-I = 0.48$; for VA 407, $V = 10.48$, $B-V = 1.14$, $V-R = 0.62$, $R-I = 0.42$.

The large error in $V-R$ results from the fact that both V and R were derived as magnitudes, and the color computed subsequently, while $B-V$ and $R-I$ were reduced as colors. Otherwise, the external comparison is about as expected, and the derived errors are quite comparable to those calculated by Weis and Upgren (1982) for their recent M dwarf survey obtained with the same telescopes and detectors. Some of the apparent spread in the V-magnitudes is not due to errors in the photometry, but reflects the fact that many M dwarfs are small-amplitude, photometric variables. Among the stars observed by us at *BVRI*, GL 15B, GL 176, GL 277A, GL 285, GL 406, GL 410, GL 494, GL 875.1, and GL 905 are known variables (Bopp and Espenak 1977; Bopp *et al.* 1983; Chugainov 1974; Eggen 1971; Kron 1950; Krzeminski 1969). Bopp and Espenak (1977) noted GL 22 as possibly variable, on the basis of a relatively large difference between their photometry and previously published data. Our own photometry confirms the variability of GL 15B, GL 285, and GL 905, with a range in V-magnitude of 0.04 mag for each star. We also appear to confirm the variability of GL 22AB, since we find $V = 10.26$ (in 1983) compared with $V = 10.30$ (in 1975, as listed by Bopp and Espenak) and $V = 10.34$ (prior to 1969). Other stars which we identify as variable on the basis of our own photometry are GL 213, GL 402, and GL 473, with a range in V of 0.08, 0.04, and 0.05 mag, respectively. Our photometry differs from Eggen's by 0.1 mag or more for GL 471 and GL 831, and those stars may be variable.

b) *Infrared Photometry*

Infrared photometry for the Gliese catalog sample was obtained during observing runs at Kitt Peak during 1983 January and 1984 April. Two different sets of instrumentation were used, HERMANN and the 2.1 m telescope in 1983 and OTTO and the 1.3 m telescope in 1984 (Goad 1982). Standard stars were selected from Elias *et al.* (1982) and Frogel *et al.* (1978), and our final photometry is thus calibrated on the "CIT" system as defined by the standard stars in those two papers. Our new *JHK* photometry is provided in Table 1, columns (7), (8), and (9) being the K, $J-H$, and $H-K$ magnitudes, respectively.

All of the program stars are relatively bright in the infrared, and it was always possible to obtain a sufficient signal-to-noise ratio for better than 1% photometry in each filter. Observations of the same star taken consecutively often differed by only a few thousandths of a magnitude. However, comparison of photometry obtained on different nights or during different observing runs showed a 1 σ scatter of about 0.015 mag for J, $J-H$, and $H-K$. We attribute much of that scatter either to slight variations in the transparency or to drifts in the detector.

The best external check on the accuracy of our photometry comes from comparison with the M dwarf photometry of Persson, Aaronson, and Frogel (1977), who used the same set of standards that we did, and Mould and Hyland (1976), who used standards from Glass (1974). The results for those two

TABLE 1

NEW PHOTOMETRIC AND SPECTROSCOPIC DATA FOR NEARBY M DWARFS

GLIESE	OTHER	V	B-V	V-R	R-I	K	J-H	H-K	CZ	Hα[a]	σ[b]	NUMBER[c]
GL2	V 216	9.93	1.49	1.05	0.85	0.000	0.000	0.000	0.8	-0.45	0.32	1 0 1
GL15A	Y 49A	0.00	0.00	0.00	0.00	0.000	0.000	0.000	9.6	-0.28	0.25	0 0 2
GL15B	GQ AND	11.08	1.79	1.46	1.26	0.000	0.000	0.000	9.7	0.00	0.00	14 0 1
GL22AB	Y 86	10.26	1.56	1.14	0.99	0.000	0.000	0.000	-5.0	-0.14	0.13	0 0 2
GL26	Y 107	11.05	1.52	1.15	1.01	0.000	0.000	0.000	-1.2	-0.36	0.29	1 0 3
GL37AB	Y 166	9.16	1.51	1.03	0.83	0.000	0.000	0.000	0.0	0.00	0.00	1 0 0
GL38	Y 169	10.65	1.39	0.91	0.70	0.000	0.000	0.000	-16.6	-0.33	0.00	1 0 0
GL47	Y 205	10.83	1.56	1.14	0.99	0.000	0.000	0.000	7.7	-0.34	0.27	1 0 2
GL48	Y 202	10.00	1.44	1.18	1.08	0.000	0.000	0.000	-0.2	-0.36	0.00	1 0 1
GL49	Y 204	9.55	1.48	1.05	0.87	0.000	0.000	0.000	-5.0	-0.27	0.27	1 0 2
GL56.3	Y 269	10.70	1.40	0.87	0.62	0.000	0.000	0.000	19.0	-0.54	0.00	1 0 2
GL63AB	Y 334	11.19	1.39	0.95	0.86	0.000	0.000	0.000	-18.5	-0.29	0.24	1 0 1
GL70	Y 363.1	10.91	1.53	1.14	1.01	0.000	0.000	0.000	-25.2	-0.27	0.25	1 0 1
GL82	Y 408	12.24	1.56	1.46	1.30	0.000	0.000	0.000	-9.8	4.73	0.51	1 0 3
GL87	Y 450	10.04	1.43	1.00	0.86	0.000	0.000	0.000	0.0	0.00	0.00	9 0 0
GL96	Y 481	0.00	0.00	0.00	0.00	0.000	0.000	0.000	-37.7	-0.49	0.33	0 0 2
GL98AB	Y 500	0.00	0.00	0.00	0.00	0.000	0.000	0.000	8.4	-0.59	0.40	0 0 2
GL105B	Y 520B	11.66	1.59	1.42	1.27	0.000	0.000	0.000	24.7	-0.05	0.25	21 0 1
GL109	Y 555	10.57	1.56	1.22	1.09	0.000	0.000	0.000	29.6	-0.31	0.27	1 0 2
GL119A	Y 602A	10.46	1.40	0.96	0.79	0.000	0.000	0.000	75.6	-0.47	0.34	1 0 1
GL119B	Y 602B	11.65	1.43	1.17	1.04	0.000	0.000	0.000	0.0	0.00	0.00	1 0 0
GL125	Y 652	10.15	1.47	1.08	0.92	0.000	0.000	0.000	-10.3	0.00	0.00	1 0 1
GL130.1A	Y 669A	0.00	0.00	0.00	0.00	0.000	0.000	0.000	21.0	-0.46	0.32	0 0 1
GL130.1B	Y 669B	0.00	0.00	0.00	0.00	0.000	0.000	0.000	21.1	-0.38	0.25	0 0 1
GL133	Y 659	11.18	1.54	1.11	0.96	0.000	0.000	0.000	-11.2	-0.37	0.33	1 0 1
GL134	Y 681	0.00	0.00	0.00	0.00	0.000	0.000	0.000	-3.8	-0.50	0.32	0 0 1
GL153A	Y 778A	0.00	0.00	0.00	0.00	0.000	0.000	0.000	3.3	-0.61	0.32	0 0 1
GL153B	Y 778B	0.00	0.00	0.00	0.00	0.000	0.000	0.000	2.1	-0.36	0.26	0 0 1
GL154	Y 808	9.60	1.45	0.95	0.72	0.000	0.000	0.000	0.0	0.00	0.00	3 0 0
GL156.1A	Y 861	10.86	1.41	1.01	0.83	0.000	0.000	0.000	0.0	0.00	0.00	1 0 0
GL157A	Y 873A	0.00	0.00	0.00	0.00	0.000	0.000	0.000	4.7	-0.73	0.44	0 0 1
GL157B	Y 873B	0.00	0.00	0.00	0.00	0.000	0.000	0.000	0.0	1.59	0.48	0 0 1
GL162	Y 913	10.16	1.51	1.00	0.83	0.000	0.000	0.000	35.8	-0.52	0.33	1 0 1
GL169	Y 990	0.00	0.00	0.00	0.00	0.000	0.000	0.000	-32.8	-0.54	0.34	0 0 1
GL169.1A	G175-34	11.08	1.64	1.45	1.28	0.000	0.000	0.000	0.0	0.00	0.00	1 0 0
GL176	Y 1046	9.98	1.51	1.13	0.97	0.000	0.000	0.000	25.1	-0.32	0.28	1 0 2
GL181	Y 1103	9.77	1.45	0.92	0.69	6.090	0.640	0.180	-32.8	-0.50	0.35	1 1 1
GL192	Y 1176	10.76	1.53	1.12	0.95	0.000	0.000	0.000	-29.6	-0.38	0.28	1 0 2
GL195A	Y 1193	10.11	1.50	1.08	0.91	5.880	0.620	0.240	30.0	-0.38	0.31	1 1 1
GL205	Y 1255	0.00	0.00	0.00	0.00	0.000	0.000	0.000	4.2	-0.47	0.34	0 0 2
GL206	V998ORI	11.52	1.63	1.36	1.20	5.610	0.580	0.270	31.2	3.17	0.55	1 1 2
GL207.1	V371ORI	11.58	1.57	1.25	1.09	0.000	0.000	0.000	21.0	4.42	0.56	1 0 3
GL212	Y 1291	9.74	1.47	1.02	0.81	5.750	0.640	0.210	1.9	-0.31	0.28	1 2 1
GL213	Y 1305	11.52	1.63	1.45	1.29	0.000	0.000	0.000	105.0	-0.21	0.21	9 0 2
GL226	Y 1358	10.50	1.51	1.18	1.01	6.020	0.570	0.250	0.0	0.00	0.00	1 1 0
GL228A	Y 1426	10.40	1.46	1.15	1.04	0.000	0.000	0.000	54.5	-0.41	0.31	12 0 1
GL234A	V577MON	11.08	1.71	1.59	1.38	0.000	0.000	0.000	15.4	3.56	0.52	5 0 1
GL239	Y 1538	9.60	1.47	0.96	0.73	0.000	0.000	0.000	-57.1	-0.40	0.29	1 0 1
GL250B	Y 1606B	10.07	1.51	1.13	0.99	0.000	0.000	0.000	-7.9	-0.41	0.31	3 0 1
GL251	Y 1609	10.00	1.55	1.25	1.12	5.270	0.600	0.250	23.3	-0.28	0.24	1 1 2
GL251.1	R 611	10.56	1.21	0.74	0.50	7.550	0.610	0.110	15.4	-0.70	0.40	1 1 3
GL268	Y 1668	11.49	1.70	1.60	1.37	5.880	0.600	0.280	65.0	1.86	0.50	14 0 4
GL270	Y 1715	10.07	1.42	0.93	0.70	6.370	0.650	0.170	-69.0	-0.52	0.32	1 1 3
GL272	V 493	10.52	1.46	1.03	0.84	6.490	0.650	0.190	0.0	0.00	0.00	1 2 2
GL273	Y 1755	9.87	1.57	1.37	1.22	4.900	0.520	0.250	19.0	0.00	0.00	1 1 2
GL277A	Y 1774A	10.56	1.46	1.20	1.08	5.940	0.620	0.230	0.1	1.35	0.55	3 1 2
GL277B	R 989	11.77	1.52	1.36	1.23	6.760	0.610	0.220	-0.9	2.15	0.50	5 1 2
GL285	YZ CMI	11.18	1.61	1.52	1.35	5.750	0.580	0.270	26.4	7.84	0.49	4 1 3
GL289	Y 1844	11.41	1.52	1.07	0.89	0.000	0.000	0.000	0.0	0.00	0.00	1 0 0
GL298	L242-66	0.00	0.00	0.00	0.00	7.410	0.520	0.220	0.0	0.00	0.00	0 1 0
GL300	Y 1953.1	12.07	1.58	1.48	1.33	0.000	0.000	0.000	0.0	0.00	0.00	1 0 0
GL310	Y 2037	0.00	0.00	0.00	0.00	5.540	0.640	0.170	10.6	-0.53	0.30	0 1 2
GL317	Y 2076.1	11.95	1.53	1.33	1.20	0.000	0.000	0.000	0.0	0.00	0.00	1 0 0
GL318.1	Y 2076	14.11	1.63	1.20	1.03	0.000	0.000	0.000	0.0	0.00	0.00	1 0 0
GL319A	Y 2078A	9.61	1.41	0.95	0.73	5.880	0.660	0.180	28.2	-0.55	0.33	1 1 3
GL319C	Y 2078C	11.76	1.54	1.19	1.05	7.300	0.600	0.230	21.4	-0.35	0.32	3 1 1
GL326AB	Y 2128	11.91	1.61	1.26	1.12	0.000	0.000	0.000	0.0	0.00	0.00	1 0 0
GL328	Y 2132	9.96	1.38	0.90	0.67	6.420	0.660	0.150	-4.1	-0.61	0.37	1 1 3
GL330	V 260	10.59	1.51	1.05	0.85	6.560	0.590	0.220	-13.1	-0.41	0.31	1 1 2
GL333.2A	Y 2154.1A	12.31	1.45	1.20	1.09	0.000	0.000	0.000	-38.1	-0.35	0.28	2 0 1
GL333.2B	R 687	12.69	1.46	1.24	1.15	0.000	0.000	0.000	-38.0	-0.28	0.23	1 0 1
GL336	V 540	9.96	1.36	0.93	0.71	6.270	0.600	0.190	9.1	-0.51	0.35	2 3 5
GL343	Y 2240	13.43	1.61	1.07	0.95	0.000	0.000	0.000	0.0	0.00	0.00	1 0 1
GL347A	Y 2254A	12.10	1.51	1.20	1.06	0.000	0.000	0.000	7.5	-0.28	0.25	1 0 1
GL350B	L1398-24	14.30	1.59	1.23	1.06	0.000	0.000	0.000	0.0	0.00	0.00	4 0 0
GL351.1	Y 2263	12.22	1.50	1.11	0.97	0.000	0.000	0.000	0.0	0.00	0.00	1 0 0
GL353	Y 2262	10.20	1.47	0.99	0.78	6.340	0.600	0.210	19.5	-0.40	0.29	2 4 5
GL359	Y 2295	14.26	1.79	1.57	1.37	0.000	0.000	0.000	0.0	0.00	0.00	2 0 0
GL360	Y 2291	10.56	1.50	1.15	1.02	6.050	0.620	0.230	5.9	-0.16	0.21	1 1 1
GL361	Y 2298	10.36	1.50	1.10	0.94	6.170	0.600	0.230	10.1	-0.35	0.26	3 1 2
GL362	Y 2292	11.22	1.52	1.27	1.13	6.430	0.620	0.240	5.0	0.80	0.51	5 1 3
GL363	Y 2294	12.51	1.53	1.35	1.22	0.000	0.000	0.000	0.0	0.00	0.00	1 0 0
GL366	Y 2302	10.63	1.40	1.03	0.86	6.600	0.600	0.200	-28.8	-0.47	0.30	4 1 1
GL373	Y 2345	0.00	0.00	0.00	0.00	5.210	0.680	0.130	13.8	-0.49	0.33	0 1 3
GL378	Y 2370.1	10.07	1.37	0.98	0.82	6.150	0.640	0.180	-10.8	-0.50	0.34	3 1 4
GL382	V 569	9.25	1.46	1.10	0.92	0.000	0.000	0.000	6.7	-0.37	0.30	1 1 2
GL388	AD LEO	9.37	1.53	1.26	1.13	0.000	0.000	0.000	12.0	3.43	0.50	1 0 5
GL393	Y 2456	9.64	1.50	1.12	0.97	0.000	0.000	0.000	6.5	-0.35	0.26	1 0 1
GL399	Y 2495	11.28	1.53	1.16	1.01	0.000	0.000	0.000	0.0	0.00	0.00	1 0 0
GL400A	Y 2509.1	9.25	1.40	0.94	0.70	5.550	0.620	0.170	-4.8	-0.43	0.35	1 1 4
GL401	Y 2512	11.03	1.42	0.95	0.77	0.000	0.000	0.000	0.0	0.00	0.00	1 0 0
GL402	Y 2524	11.65	1.64	1.43	1.26	6.415	0.605	0.270	-1.8	-0.19	0.21	18 5 4
GL403	Y 2526	12.68	1.65	1.31	1.17	0.000	0.000	0.000	0.0	0.00	0.00	1 0 0
GL405	Y 2544	12.71	1.53	1.10	0.96	0.000	0.000	0.000	0.0	0.00	0.00	1 0 0
GL406	W 359	13.46	1.99	2.29	1.76	6.080	0.635	0.371	0.0	0.00	0.00	14 3 0
GL408	Y 2561	10.02	1.54	1.20	1.05	5.540	0.590	0.240	2.0	-0.38	0.27	1 2 3
GL410	Y 2574	9.57	1.46	0.98	0.77	5.720	0.660	0.190	-14.8	-0.14	0.26	1 2 5
GL411	LA21185	0.00	0.00	0.00	0.00	3.353	0.544	0.205	-84.9	-0.28	0.24	0 2 4
GL412A	Y 2582	0.00	0.00	0.00	0.00	4.760	0.569	0.212	67.9	-0.33	0.28	0 2 4
GL412B	WX UMA	14.36	1.92	2.07	1.68	0.000	0.000	0.000	0.0	0.00	0.00	3 0 0
GL414A	Y 2600A	0.00	0.00	0.00	0.00	5.023	0.628	0.130	-15.7	-0.68	0.41	0 3 4
GL414B	LFT 768	9.96	1.47	1.07	0.92	5.766	0.637	0.200	-15.1	-0.42	0.29	3 2 4
GL414.1AB	Y2600.1AB	10.89	1.50	1.19	1.06	6.341	0.612	0.223	-11.5	-0.36	0.27	1 2 3
GL420B	Y 2611B	8.07	1.66	0.89	0.71	3.978	0.834	0.168	7.6	-0.24	0.26	1 1 2
GL424	SZ UMA	9.27	1.40	0.94	0.75	5.547	0.579	0.185	58.2	-0.40	0.29	1 2 1
GL429.2	Y 2651.1	12.37	1.47	1.03	0.82	0.000	0.000	0.000	0.0	0.00	0.00	2 0 0
GL430.1	Y 2664	10.28	1.48	1.03	0.81	6.333	0.637	0.188	-6.1	-0.44	0.30	3 1 4
GL436	Y 2704.1	10.66	1.52	1.19	1.06	6.100	0.591	0.235	8.8	-0.35	0.26	3 2 5
GL443	Y 2724.1	11.75	1.50	1.24	1.09	0.000	0.000	0.000	0.0	0.00	0.00	2 0 0
GL445	Y 2722	10.82	1.58	1.33	1.20	5.930	0.510	0.250	-113.2	-0.25	0.21	5 2 5
GL447	FI VIR	11.14	1.75	1.56	1.35	5.660	0.568	0.287	-31.9	0.01	0.00	15 5 5
GL450	V 135	9.72	1.50	1.05	0.88	5.644	0.597	0.209	-0.6	-0.33	0.28	12 6 5
GL452	Y 2747.1	11.87	1.52	1.17	1.01	7.447	0.610	0.215	25.7	-0.40	0.28	4 1 4
GL452.1	Y 2750.1	12.77	1.66	1.36	1.19	0.000	0.000	0.000	0.0	0.00	0.00	1 0 0
GL455	Y 2776	12.85	1.74	1.26	1.09	0.000	0.000	0.000	0.0	0.00	0.00	1 0 0
GL456	Y 2795	11.25	1.40	0.92	0.69	7.600	0.631	0.171	3.9	-0.50	0.33	4 2 2
GL458A	Y 2811	9.71	1.44	0.96	0.75	6.080	0.644	0.159	-18.6	-0.47	0.30	1 2 4
GL458.2	V 640	10.52	1.43	0.95	0.72	6.797	0.648	0.164	-17.4	-0.36	0.26	2 2 1
GL459.3	Y 2838	10.61	1.44	0.95	0.75	6.839	0.658	0.156	-3.1	-0.36	0.24	6 2 4
GL463	Y 2853	11.58	1.45	1.16	1.05	7.128	0.602	0.209	6.7	-0.32	0.25	2 2 4
GL464	Y 2853.1	10.37	1.41	0.93	0.72	6.690	0.658	0.155	5.1	-0.53	0.33	2 2 4
GL471	Y 2885	9.68	1.44	0.94	0.72	5.949	0.646	0.167	17.7	-0.47	0.33	1 3 5
GL473AB	W 424AB	12.47	1.83	1.92	1.58	6.073	0.573	0.327	0.0	0.00	0.00	10 3 0
GL476	Y 2901	11.41	1.41	1.10	0.99	7.145	0.575	0.211	31.6	-0.41	0.28	2 2 3
GL480	Y 2915	11.50	1.48	1.27	1.14	6.693	0.618	0.241	-5.8	-0.32	0.26	2 2 3
GL486	Y 2943	11.38	1.56	1.37	1.23	6.377	0.578	0.249	17.6	-0.29	0.30	9 1 2
GL487	Y 2949	10.91	1.63	1.32	1.16	6.093	0.564	0.249	-4.1	0.28	0.50	2 2 7
GL488	Y 2951	0.00	0.00	0.00	0.00	4.940	0.672	0.148	2.9	-0.59	0.38	0 1 4

TABLE 1—*Continued*

GLIESE	OTHER	V	B-V	V-R	R-I	K	J-H	H-K	CZ	Hα[a]	σ[b]	NUMBER[c]
GL490A	V 298	0.00	0.00	0.00	0.00	0.000	0.000	0.000	-9.0	1.65	0.50	0 0 3
GL490B	+36 2322B	0.00	0.00	0.00	0.00	0.000	0.000	0.000	-3.8	3.65	0.65	0 0 2
GL494	V 140	9.78	1.46	1.04	0.87	5.613	0.660	0.190	-13.1	2.12	0.51	1 3 3
GL507A	V 46	0.00	0.00	0.00	0.00	0.000	0.000	0.000	-16.0	-0.36	0.37	0 0 1
GL507B	Y 3047B	0.00	0.00	0.00	0.00	0.000	0.000	0.000	-9.8	0.01	0.00	0 0 1
GL507.1	Y 3047.1	10.60	1.48	1.06	0.90	6.425	0.662	0.193	-13.5	-0.48	0.31	4 1 3
GL508AB	Y 3048.1	0.00	0.00	0.00	0.00	4.500	0.618	0.191	-4.3	-0.31	0.28	0 1 4
GL512A	R 486A	11.30	1.51	1.25	1.12	6.411	0.626	0.241	-42.6	-0.33	0.26	6 1 4
GL512B	Y 3074B	13.75	1.70	1.54	1.34	0.000	0.000	0.000	0.0	0.00	0.00	1 0 0
GL513	G63-32	12.12	1.43	1.21	1.12	7.549	0.570	0.203	0.0	0.00	0.00	2 1 0
GL514	Y 3079	9.06	1.47	1.03	0.81	5.060	0.617	0.197	13.3	-0.43	0.30	1 2 4
GL516A	VW COM	0.00	0.00	0.00	0.00	0.000	0.000	0.000	-02.9	0.01	0.00	0 0 2
GL516B	V 3094.1B	0.00	0.00	0.00	0.00	0.000	0.000	0.000	-02.5	0.01	0.00	0 0 2
GL519	Y 3116.1	9.00	1.43	0.89	0.65	5.495	0.629	0.157	-16.4	-0.46	0.33	1 3 5
GL520C	+48 2138C	14.43	1.66	1.44	1.29	0.000	0.000	0.000	0.0	0.00	0.00	1 0 0
GL521	Y 3122.1	10.23	1.40	1.01	0.85	6.291	0.592	0.182	-67.1	-0.38	0.29	3 1 2
GL521.1	Y 3121	0.00	0.00	0.00	0.00	0.000	0.000	0.000	4.0	-0.59	0.37	0 0 1
GL522	Y 3126.1	9.75	1.29	0.79	0.55	6.530	0.632	0.109	44.9	-0.63	0.37	1 1 2
GL524.1	Y 3131.2	10.53	1.32	0.80	0.56	7.227	0.658	0.132	3.5	-0.55	0.31	1 1 2
GL525	Y 3133	9.77	1.41	0.89	0.66	6.229	0.591	0.178	19.0	-0.41	0.29	4 2 3
GL526	Y 3135	0.00	0.00	0.00	0.00	4.459	0.587	0.198	14.3	-0.45	0.30	0 1 3
GL533.1	Y 3176	11.83	1.50	1.07	0.89	7.710	0.605	0.221	-53.5	-0.37	0.27	2 1 2
GL536.1AB	Y 3198.1	10.63	1.44	0.95	0.72	6.920	0.631	0.176	-11.5	-0.45	0.33	3 2 3
GL537AB	Y 3200	0.00	0.00	0.00	0.00	5.202	0.615	0.194	-42.1	-0.31	0.28	0 1 4
GL540	Y 3237	10.35	1.40	1.01	0.83	6.388	0.667	0.166	6.4	-0.52	0.35	1 1 1
GL543	Y 3252	13.43	1.64	1.23	1.09	0.000	0.000	0.000	0.0	0.00	0.00	1 0 0
GL545	Y 3256.1	12.84	1.58	1.35	1.21	7.961	0.525	0.245	0.0	0.00	0.00	2 1 0
GL548A	Y 3273A	9.73	1.45	0.95	0.73	5.985	0.667	0.157	7.6	-0.53	0.35	1 2 4
GL548B	LFT1106	9.98	1.48	0.98	0.79	6.097	0.673	0.173	6.7	-0.52	0.34	1 1 4
GL549B	Y 3274	0.00	0.00	0.00	0.00	7.114	0.618	0.226	0.0	0.00	0.00	0 1 0
GL552	Y 3283	10.66	1.48	1.09	0.95	6.405	0.629	0.207	5.8	-0.40	0.31	3 2 3
GL555	Y 3296	11.31	1.60	1.46	1.29	5.968	0.619	0.268	0.0	0.00	0.00	4 2 0
GL563	Y 3341.1	12.07	1.50	1.05	0.86	8.041	0.614	0.201	0.0	0.00	0.00	1 1 0
GL563.1	V 884	9.74	1.34	0.80	0.57	6.525	0.629	0.119	-14.6	-0.54	0.38	1 2 3
GL568AB	Y 3369	11.68	1.59	1.39	1.23	6.569	0.611	0.264	-36.7	0.01	0.00	2 1 3
GL570.2	Y 3383	11.11	1.32	0.85	0.63	7.686	0.632	0.140	6.4	-0.37	0.30	2 3 2
GL581	Y 3458	10.55	1.58	1.26	1.11	5.849	0.597	0.249	-10.1	-0.29	0.26	1 3 2
GL585	Y 3481	13.68	1.72	1.56	1.36	8.296	0.514	0.272	0.0	0.00	0.00	1 1 0
GL586C	Y 3491C	15.41	1.64	1.66	1.42	0.000	0.000	0.000	0.0	0.00	0.00	2 0 0
GL589A	Y 3520A	12.40	1.58	1.19	1.05	7.972	0.522	0.232	-44.2	-0.21	0.24	1 1 1
GL589B	Y 3520B	15.00	1.84	1.63	1.41	0.000	0.000	0.000	0.0	0.00	0.00	1 0 0
GL597	Y 3575	12.19	1.63	1.28	1.12	7.466	0.583	0.246	-47.1	-0.23	0.22	1 1 1
GL 607	Y 3630	0.00	0.00	0.00	0.00	7.834	0.582	0.257	9.1	-0.31	0.25	0 1 1
GL611.3	G16-29	11.54	1.44	1.01	0.85	7.519	0.648	0.190	-42.2	-0.45	0.31	1 1 4
GL616.2	CR DRA	9.97	1.49	1.07	0.90	5.771	0.667	0.184	-33.6	1.81	0.55	2 1 4
GL617A	V 162	0.00	0.00	0.00	0.00	4.994	0.671	0.145	-21.3	-0.58	0.37	0 2 2
GL617B	Y 3712B	10.68	1.49	1.20	1.08	6.093	0.619	0.224	-20.5	-0.31	0.28	1 1 2
GL618.1	V 760	10.66	1.37	0.88	0.68	7.105	0.673	0.148	-119.1	-0.62	0.35	1 3 2
GL623	Y 3733	10.26	1.50	1.13	1.02	5.912	0.526	0.226	-29.2	-0.21	0.19	1 2 1
GL625	V 767	10.10	1.60	1.12	0.95	5.837	0.570	0.225	-13.5	-0.30	0.25	1 2 3
GL642	Y 3841	10.74	1.41	0.92	0.70	7.102	0.602	0.188	-68.3	-0.49	0.31	1 1 3
GL643	Y 3844	11.75	1.68	1.40	1.22	6.743	0.559	0.265	15.1	-0.26	0.22	1 1 3
GL644AB	V10540PH	0.00	0.00	0.00	0.00	4.393	0.645	0.235	11.1	1.73	0.67	0 2 2
GL644C	Y 3845C	0.00	0.00	0.00	0.00	8.803	0.589	0.374	0.0	0.00	0.00	0 1 0
GL649	Y 3857	9.68	1.50	1.03	0.84	5.640	0.630	0.195	2.5	-0.33	0.27	8 3 3
GL654	Y 3880	0.00	0.00	0.00	0.00	5.971	0.583	0.201	0.9	-0.40	0.28	0 3 1
GL655	Y 3889	11.62	1.54	1.20	1.08	7.046	0.600	0.233	-50.9	-0.32	0.23	3 4 2
GL661AB	Y 3907	0.00	0.00	0.00	0.00	4.824	0.521	0.223	-31.8	-0.20	0.20	0 1 3
GL668AB	V 792	0.00	0.00	0.00	0.00	6.923	0.658	0.153	0.0	0.00	0.00	0 1 0
GL669A	V645HER	11.43	1.55	1.35	1.21	6.432	0.624	0.239	-34.7	1.63	0.51	1 2 3
GL669B	Y 3941B	12.95	1.62	1.60	1.39	0.000	0.000	0.000	-35.0	5.67	0.51	1 1 1
GL671	Y 3944	11.37	1.55	1.17	1.04	6.913	0.573	0.227	-19.9	-0.28	0.25	1 3 2
GL678.1	Y 3975.1	0.00	0.00	0.00	0.00	5.459	0.643	0.188	-14.0	-0.54	0.35	0 3 1
GL685	Y 4017	0.00	0.00	0.00	0.00	6.083	0.658	0.175	-17.1	-0.40	0.31	0 1 2
GL686	Y 4009	0.00	0.00	0.00	0.00	5.584	0.595	0.210	-12.2	-0.38	0.30	0 2 1
GL687	Y 4029	0.00	0.00	0.00	0.00	4.520	0.574	0.221	0.0	0.00	0.00	0 1 0
GL694	Y 4053	10.48	1.53	1.16	1.03	6.004	0.611	0.225	-17.8	-0.34	0.30	1 3 1
GL694.2	Y 4062	10.71	1.47	0.99	0.78	6.831	0.647	0.181	4.7	-0.40	0.31	1 3 2
GL696	Y 4074	0.00	0.00	0.00	0.00	6.529	0.672	0.152	-26.7	-0.53	0.31	0 1 1
GL699	Y 4098	0.00	0.00	0.00	0.00	4.558	0.504	0.265	0.0	0.00	0.00	0 1 0
GL701	Y 4133	0.00	0.00	0.00	0.00	5.335	0.595	0.216	30.2	-0.44	0.28	0 1 1
GL708	Y 4192	10.02	1.32	0.77	0.54	6.837	0.629	0.122	1.1	-0.70	0.37	0 2 1
GL710	Y 4204	0.00	0.00	0.00	0.00	6.302	0.658	0.134	-14.3	-0.56	0.32	0 1 1
GL712	Y 4221	0.00	0.00	0.00	0.00	7.910	0.506	0.220	0.0	0.00	0.00	0 2 0
GL720A	V 182	0.00	0.00	0.00	0.00	6.111	0.658	0.157	-31.8	-0.50	0.32	0 1 4
GL720B	Y 4285B	13.00	1.60	1.36	1.22	8.090	0.551	0.244	0.0	0.00	0.00	1 1 0
GL725A	V 184	0.00	0.00	0.00	0.00	4.443	0.529	0.223	-3.0	-0.22	0.23	0 1 3
GL725B	Y 4330B	0.00	0.00	0.00	0.00	4.967	0.518	0.237	-0.9	-0.21	0.20	0 1 3
GL728	Y 4345	0.00	0.00	0.00	0.00	5.871	0.651	0.120	-24.0	0.00	0.00	0 1 1
GL730	Y 4348	10.72	1.45	0.97	0.78	6.859	0.655	0.173	-2.4	-0.39	0.30	1 1 1
GL731	Y 4356	10.10	1.47	0.96	0.72	6.340	0.639	0.184	-15.9	-0.49	0.29	0 1 2
GL735	V1285AQL	10.10	1.53	1.24	1.09	5.417	0.628	0.224	-12.6	1.69	0.54	0 1 1
GL740	Y 4398	0.00	0.00	0.00	0.00	5.371	0.659	0.176	9.3	-0.55	0.34	0 1 2
GL745A	R 730	10.76	1.59	1.11	0.96	6.525	0.561	0.224	30.7	-0.22	0.22	1 1 3
GL745B	R 731	10.75	1.58	1.11	0.96	6.509	0.555	0.225	29.7	-0.23	0.22	1 1 2
GL747AB	Y 4459	11.26	1.68	1.33	1.17	6.433	0.558	0.257	-48.0	-0.27	0.25	1 2 1
GL752A	V 65	0.00	0.00	0.00	0.00	4.660	0.625	0.215	35.4	-0.35	0.28	0 2 4
GL752B	Y 4494B	0.00	0.00	0.00	0.00	8.806	0.674	0.436	0.0	0.00	0.00	0 1 0
GL756	Y 4535	11.53	1.42	1.01	0.87	7.552	0.596	0.185	-31.6	-0.37	0.25	1 1 1
GL761.2	Y 4573	10.41	1.42	0.90	0.68	6.843	0.654	0.149	-48.9	-0.51	0.37	1 1 1
GL763	Y 4583	0.00	0.00	0.00	0.00	5.901	0.651	0.144	-59.1	-0.59	0.34	0 1 1
GL766AB	Y 4646	12.38	1.67	1.48	1.31	7.144	0.559	0.277	0.0	0.00	0.00	1 1 0
GL767A	Y 4652A	9.77	1.48	1.05	0.89	5.647	0.628	0.202	-5.4	-0.44	0.32	1 1 2
GL777	Y 4756	14.38	1.59	1.62	1.41	0.000	0.000	0.000	-5.0	-0.32	0.29	1 0 0
GL781	Y 4775	11.97	1.56	1.02	0.82	8.094	0.524	0.213	-149.0	1.22	0.53	1 1 1
GL793	Y 4889	10.54	1.56	1.22	1.09	5.945	0.600	0.230	8.9	-0.04	0.00	1 1 1
GL804	Y 4945	10.30	1.42	0.95	0.74	6.552	0.631	0.176	2.0	-0.43	0.28	1 1 1
GL806	Y 4951	10.77	1.53	1.10	0.94	6.578	0.589	0.215	-26.6	-0.35	0.27	1 1 1
GL812A	Y 5016	0.00	0.00	0.00	0.00	7.088	0.542	0.221	-45.5	1.74	0.45	0 1 2
GL813	Y 5024	12.01	1.60	1.15	1.01	7.680	0.556	0.233	-32.1	-0.22	0.26	1 1 1

TABLE 1—*Continued*

GLIESE	OTHER	V	B-V	V-R	R-I	K	J-H	H-K	CZ	Hα[a]	σ[b]	NUMBER[c]
GL815AB	V1396CYG	0.00	0.00	0.00	0.00	5.924	0.603	0.204	7.7	1.28	0.51	0 1 2
GL828.1	Y 5164	0.00	0.00	0.00	0.00	7.015	0.678	0.132	-5.7	-0.58	0.32	0 1 1
GL829	Y 5177	10.31	1.61	1.31	1.16	5.476	0.580	0.248	-25.9	-0.17	0.22	4 1 1
GL831	Y 5184	12.03	1.68	1.57	1.37	0.000	0.000	0.000	-49.6	1.37	0.44	2 0 1
GL839	Y 5292	10.34	1.35	0.86	0.66	6.810	0.667	0.127	-49.0	-0.67	0.35	1 1 3
GL844	Y 5317	10.64	1.51	1.16	1.01	6.224	0.644	0.213	-15.8	-0.26	0.27	0 1 3
GL849	Y 5358	0.00	0.00	0.00	0.00	0.000	0.000	0.000	-15.9	-0.41	0.29	0 0 1
GL851	Y 5367	10.21	1.49	1.13	0.97	5.849	0.685	0.202	-52.3	-0.31	0.26	0 1 1
GL860AB	KR60AB	0.00	0.00	0.00	0.00	4.711	0.581	0.249	-34.2	0.01	0.00	0 1 1
GL873	EV LAC	10.26	1.58	1.36	1.20	5.312	0.587	0.236	-1.4	3.36	0.56	1 1 2
GL875	Y 5527	9.81	1.46	0.94	0.71	0.000	0.000	0.000	-7.0	-0.47	0.28	0 1 1
GL875.1	GT PEG	11.61	1.50	1.24	1.10	6.905	0.639	0.228	-4.0	3.58	0.53	1 0 2
GL880	Y 5563	0.00	0.00	0.00	0.00	0.000	0.000	0.000	0.0	-0.45	0.31	0 0 1
GL894.1	Y 5639	10.90	1.45	0.96	0.76	0.000	0.000	0.000	-6.7	-0.41	0.31	1 0 1
GL895	Y 5665	10.01	1.49	1.00	0.86	0.000	0.000	0.000	-34.8	-0.34	0.28	1 0 1
GL896A	EQ PEG A	0.00	0.00	0.00	0.00	0.000	0.000	0.000	0.1	4.26	0.59	0 0 2
GL896B	EQ PEG B	0.00	0.00	0.00	0.00	0.000	0.000	0.000	0.4	5.11	0.55	0 0 3
GL899	Y 5699	11.16	1.47	1.11	1.00	0.000	0.000	0.000	0.0	0.00	0.00	1 0 0
GL900	Y 5703.1	9.52	1.34	0.84	0.62	0.000	0.000	0.000	-11.9	0.01	0.00	0 0 4
GL905	Y 5736	12.30	1.88	1.87	1.53	0.000	0.000	0.000	0.0	0.00	0.00	16 0 0
GL905.2A	G130-6	11.68	1.57	1.22	1.09	0.000	0.000	0.000	-25.3	-0.36	0.26	1 0 1
GL908	Y 5763	0.00	0.00	0.00	0.00	0.000	0.000	0.000	-71.2	-0.40	0.28	0 0 3
W9431B	Y 3010B	12.30	1.30	0.84	0.63	0.000	0.000	0.000	0.0	0.00	0.00	1 0 0
W9443	Y 3058	11.81	1.38	0.96	0.76	0.000	0.000	0.000	0.0	0.00	0.00	1 0 0
W9447	Y 3080	14.24	1.65	1.57	1.37	0.000	0.000	0.000	0.0	0.00	0.00	1 0 0
W9484	Y 3285.1	11.90	1.57	1.33	1.19	0.000	0.000	0.000	0.0	0.00	0.00	1 0 0
W9486	Y 3294.1	10.53	1.24	0.76	0.54	0.000	0.000	0.000	0.0	0.00	0.00	1 0 0
W9495A	Y 3346A	11.65	1.47	1.04	0.85	0.000	0.000	0.000	0.0	0.00	0.00	1 0 0
W9495B	Y 3346B	12.05	1.50	1.08	0.91	0.000	0.000	0.000	0.0	0.00	0.00	1 0 0
W9509	Y 3405	12.75	1.52	1.13	0.98	0.000	0.000	0.000	0.0	0.00	0.00	1 0 0
W9522A	V 745	10.39	1.27	0.76	0.52	0.000	0.000	0.000	0.0	0.00	0.00	1 0 0
W9522B		14.55	1.63	1.30	1.18	0.000	0.000	0.000	0.0	0.00	0.00	1 0 0

[a] Hα equivalent width, in angstroms.
[b] Gaussian sigma for Hα, in angstroms.
[c] Number = Number of times the star was observed at *BVRI*, at *JHK*, and with the echelle spectrograph, respectively.

comparisons are as follows:

$$\langle K_{SH} - K_{PAF} \rangle = -0.009, \quad \sigma = 0.023, \quad N = 13,$$

$$\langle (J-H)_{SH} - (J-H)_{PAF} \rangle = 0.007, \quad \sigma = 0.017,$$

$$\langle (H-K)_{SH} - (H-K)_{PAF} \rangle = -0.010, \quad \sigma = 0.007,$$

$$\langle K_{SH} - K_{MH} \rangle = 0.023, \quad \sigma = 0.025, \quad N = 10,$$

$$\langle (J-H)_{SH} - (J-H)_{MH} \rangle = -0.008, \quad \sigma = 0.032,$$

$$\langle (H-K)_{SH} - (H-K)_{MH} \rangle = -0.011, \quad \sigma = 0.010,$$

The comparisons show adequate agreement, and indicate that our photometry is generally accurate to within 1%–2%. With the limited data available, it is impossible for us to say whether any of the program stars are variable in the infrared.

c) *Echelle Spectroscopy*

High-dispersion spectra for the program stars were obtained using the 1.5 m telescope and the Multiple Mirror Telescope on Mount Hopkins, and the 1.5 m Oak Ridge telescope at Harvard, Massachusetts. The echelle spectrographs and photon-counting, intensified Reticon detectors varied only slightly with time and from site to site, and the spectroscopic results from the three sites have been combined without any zero-point corrections. Since we used a one-dimensional detector, only one order of the echelle spectra was recorded for each observation. Two different echelle setups were used for the program, one with central wavelength $\lambda_c = 5200$ Å to sample the forest of strong atomic lines near Mg I *b* (Latham 1985), and one with $\lambda_c = 6563$ Å to measure Hα equivalent widths. The instrumental resolution for the two wavelength regions is FWHM $\approx$ 0.12 Å at 5200 Å and FWHM $\approx$ 0.15 Å at 6563 Å.

Reduction of the raw spectra to a wavelength scale and the derivation of radial and rotational velocities via cross-correlation techniques have been accomplished in the standard manner, following the precepts of Tonry and Davis (1979), as described elsewhere (Stauffer *et al.* 1984). The template stars utilized were GL 526 (assumed heliocentric radial velocity = +14.1 km s^{-1}) and HD 3765 (radial velocity = −63.0 km s^{-1}).

Equivalent widths for Hα were calculated both from Gaussian fits and from simple integrations of the observed counts over the line profile. The two methods agree to within a few hundredths of an angstrom, except for weak lines and stars with Hα in emission, where the profiles are far from Gaussian. The results of the spectroscopic program are given in Table 1, in the order heliocentric radial velocity, Hα equivalent width, and Gaussian sigma. The listed equivalent widths are those derived from the integration method.

On the basis of our experience with other stellar programs (Stauffer *et al.* 1984; Stauffer, Hartmann, and Jones 1985), we expect our radial velocities to have 1 σ errors of about 1 km s^{-1}. Estimating the accuracy of our velocities either from internal comparisons or from comparison with other published surveys is complicated by the likelihood that some of the stars are spectroscopic binaries. For the 35 stars for which we have four or more radial velocity determinations, the median standard deviation of the measured velocities is 0.90 km s^{-1}. The median was chosen as one way of deemphasizing the tail of the distribution which might harbor the spectroscopic binaries. A slightly more sophisticated analysis comparing the distribution of observed standard deviations with the distribution for a model population gives essentially the same estimate for our radial velocity accuracy. Three stars with standard deviations greater than 2 km s^{-1} are likely radial velocity variables (GL 487, GL 508AB, and GL 900). Note, however, that B. Bopp (1985, private communication) finds GL 900 not to be a radial velocity variable. The cross-correlation profile for GL 487 is double-peaked, indicating that it is an SB2. We also see double-peaked cross-correlation profiles or double-peaked Hα emission for GL 268, GL 616.2, GL 644AB, and GL 815AB. All but GL 487 and GL 616.2 were previously known to be spectroscopic binaries (Gliese 1969; Pettersen, Evans, and Coleman 1984; Weis 1982; and Fekel, Bopp, and Lacy 1978). Conversely, GL 402, GL 611.3, and GL 643 are listed in Gliese (1969*a*) as having variable velocities, with a range of about 35 km s^{-1} in each case, whereas our velocities over about a 1 year time span (four spectra per star) are essentially constant.

No published M dwarf radial velocity survey claims accuracies comparable to ours, so we cannot make a stringent external test of our velocity accuracy. The best comparison is with Wilson (1967), whose velocities have claimed accuracies ranging from 0.5 to 5 km s^{-1}. Excluding several stars with very large differences, for 48 stars in common we find $\langle v_{SH} - v_W \rangle = -1.73$ km s^{-1}, $\sigma = 2.9$ km s^{-1}. We believe that this is primarily a measure of Wilson's radial velocity accuracy (simply reflecting the evolution in detectors and software for radial velocity determination over the last two decades).

Projected rotational velocities may also be derived from the cross-correlation analysis. However, most of the observed stars have rotational velocities that are below our detection limit of about 10 km s^{-1}. Furthermore, none of the program stars have rotational velocities that exceed 25 km s^{-1}. For the small number of stars for which the cross-correlation profile appears to indicate detectable rotation we list our inferred $v \sin i$ in Table 8.

The accuracy of the Hα equivalent widths has been discussed previously by Young *et al.* (1986). Briefly, the signal-to-noise ratios for the spectra are such that we expect accuracies of a few hundredths of an angstrom. For the stars with Hα in emission, there is clear evidence for variability, as noted by Young *et al.*, so it is not possible to test further the accuracy of the measured equivalent widths for these stars. For the stars with Hα in absorption, we do not have enough stars with multiple Hα determinations to measure our errors directly. Instead, we have calculated the difference between the first observation and succeeding observations for all stars with two or more Hα equivalent widths. A histogram of those differences is shown in Figure 1. Only four of the pairs of observations have differences greater than 0.1 Å (GL 330, GL 548B, GL 694.2, and GL 908), and we believe that those may be the result of misidentifications at the telescope or to real

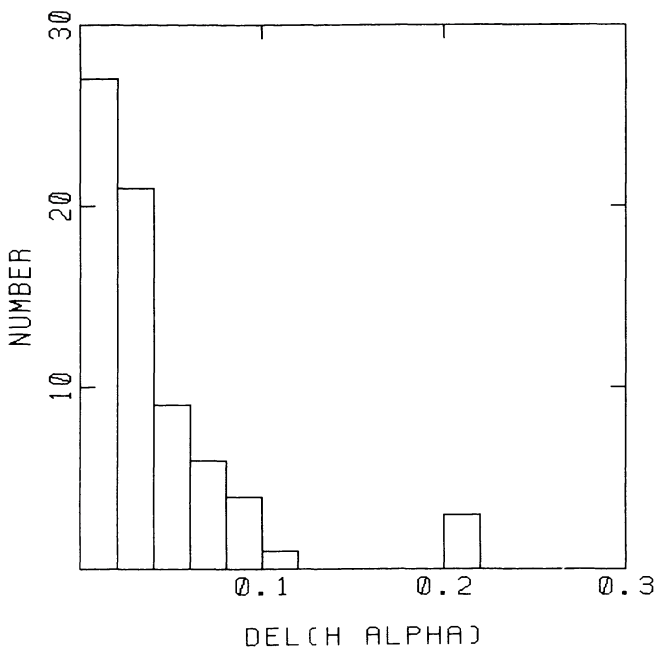

FIG. 1.—Histogram of the differences between the first and nth Hα equivalent width measurements for all stars observed more than once at Hα.

variability in the star. We note that GL 908 is listed by Joy and Abt (1974) as a dMe, so it may in fact have variable Hα (see also Young, Skumanich, and Harlan 1984). The median Hα difference for all the pairs of observations in Figure 1 is 0.03 Å.

On the basis of the small number of stars for which we have more than one high signal-to-noise Hα spectrum, the Gaussian widths (col. [12] of Table 1) for the stars with Hα in absorption appear to be accurate to 5%–10%. Because the Hα emission profiles are not, in general, well approximated by a Gaussian fit, we have instead simply estimated the heights of the emission lines and directly measured the widths at half-height.

Most of the Hα profiles for our emission-line stars show central reversals, as predicted by Cram and Mullan (1979) and observed by Worden, Schneeberger, and Giampapa (1981). However, a significant number of the stars show centrally peaked Hα profiles. As a guide to future work, we provide plots of the Hα profiles for all of our emission-line stars in Figure 2. In a few cases where we believe there is evidence for profile variability, more than one profile is shown for a given star.

d) *Narrow-Band Indices*

Low-resolution spectra for a small number of Gliese catalog M dwarfs were obtained during 1977–1980 using the Lick Observatory 0.6 m and 1.0 m telescopes. These spectra were obtained prior to (and independent of) the formulation of the general M dwarf program, and therefore the data derived from them are presented in a separate table. The detector used at Lick was an image dissector scanner (IDS), identical with the detector used for many years on the 3 m telescope (Miller, Robinson, and Wampler 1976). The wavelength range observed was generally 4700–7200 Å, at a resolution of about 7 Å. The spectra were flux-calibrated via observation of Oke (1974) and Stone (1977) standard stars.

We have extracted one set of narrow-band indices from the Lick spectra that measure the strength of three bands (due primarily to TiO) that serve as temperature indicators. Another three indices measure the strength of absorption features that are primarily gravity-sensitive. The temperature indices, $\Delta 54$, TiO59, TiO61, TiO65, compare the flux at the bottom of one of the bands to a nearby pseudo-continuum point. Precise definitions of these indices are given in Stauffer (1982*a*). The gravity indices are defined as equivalent widths, with the continuum drawn either as a straight line through two points or as a parabolic fit to four points. The specific wavelength regions defining the features and the continuum regions are shown in Table 2. Evidence that these three features are gravity-sensitive can be found in Deeming (1960), Ohman (1934), and Spinrad (1973).

The derived band indices are provided in Table 3, in the order $\Delta 54$, TiO59, TiO61, TiO65, Mg b, Na I D, Ca H, $(R-I)_{\rm TiO}$, and $(R-I)_{\rm K}$. The last two columns are the $(R-I)$ color estimated for the star from the temperature indices, as defined below, and the photometrically observed color.

The TiO indices were formulated primarily in order to derive spectroscopic estimates of the intrinsic colors for M dwarfs. An early calibration of the relation (Stauffer 1982*a*) was used to estimate the reddening of M dwarfs in the Pleiades (Stauffer 1982*b*). The same calibration was subsequently used by Mundt *et al.* (1983) to derive reddening estimates for several young stars toward the Taurus cloud. With a slightly larger sample of calibrating stars, and slightly improved measurement of the indices, we now offer a revised version of the calibrations:

$$(R-I)_{\rm K} = 0.817 + 4.163\Delta 54 - 4.303(\Delta 54)^2,$$

$$(R-I)_{\rm K} = 0.431 + 2.269{\rm TiO59} + 3.487({\rm TiO59})^2,$$

$$(R-I)_{\rm K} = 0.565 + 2.051{\rm TiO61} + 2.622({\rm TiO61})^2,$$

$$(R-I)_{\rm K} = 0.545 + 0.610{\rm TiO65} + 1.263({\rm TiO65})^2.$$

For all of the program stars, we calculate indicative $R-I$ values for each band strength, and then average the values (with equal weight) to produce the $R-I$ estimate listed in Table 3. The 1 σ dispersion of the estimated $R-I$ colors relative to the photometrically observed colors is 0.034 mag.

Since we have at most two spectra per star, we can only roughly estimate the accuracy of our measurement of the gravity indices. From examination of the eight stars with two spectra each, we believe that the 1 σ errors for the Mg b, Na I D, and Ca H indices are about 5%, 8%, and 15%, respectively.

III. CHROMOSPHERIC ACTIVITY IN M DWARFS DEDUCED FROM Hα EQUIVALENT WIDTHS

For F and G dwarfs, the most commonly used chromospheric activity indicator available in the optical part of the spectrum is the Ca II H and K lines. The Ca II H and K reversals appeal to observers as relatively strong features,

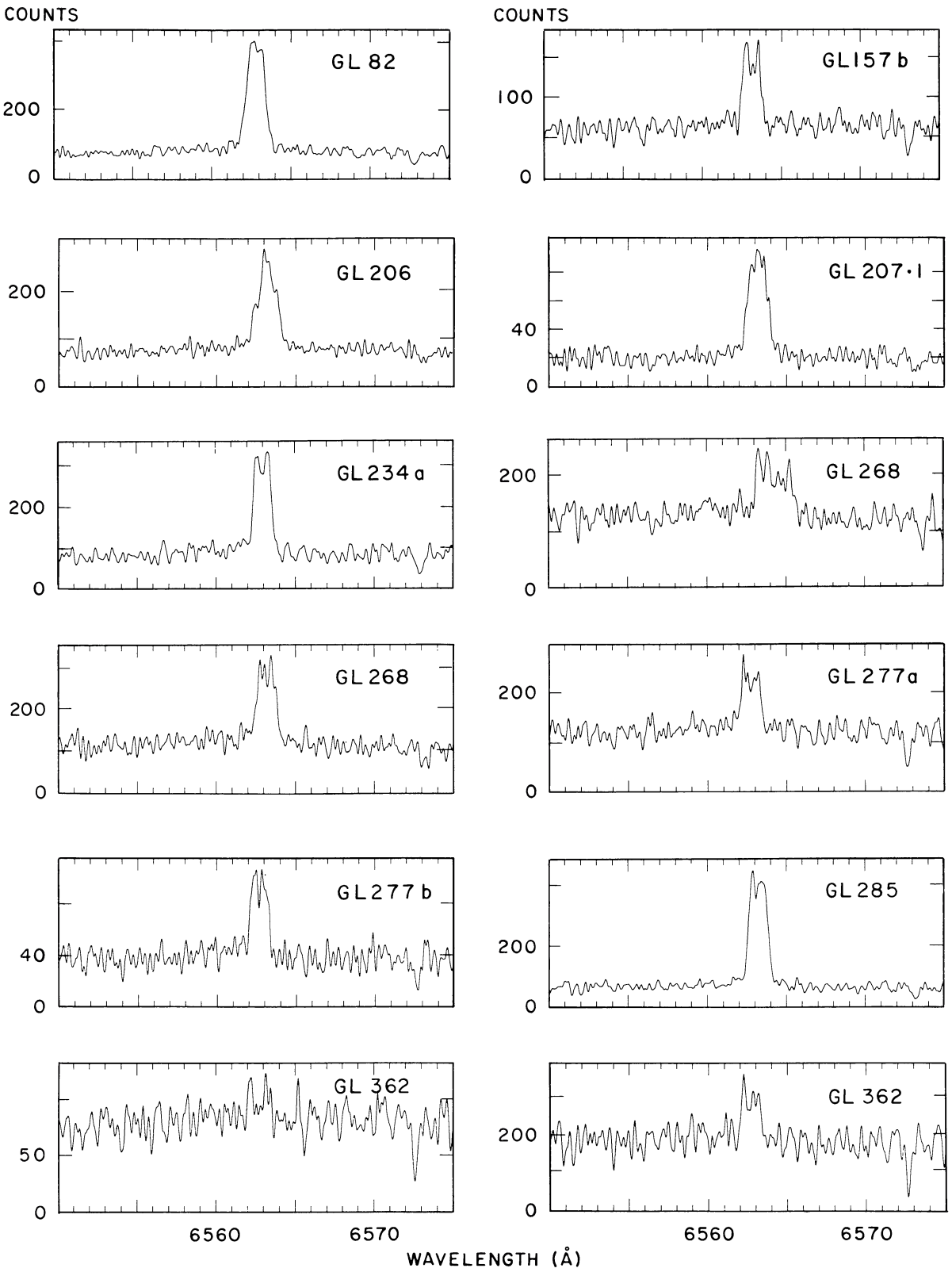

FIG. 2.—Profiles of Hα emission lines for all dMe stars in Table 1. Two Hα profiles are shown for a few stars in order to illustrate variability.

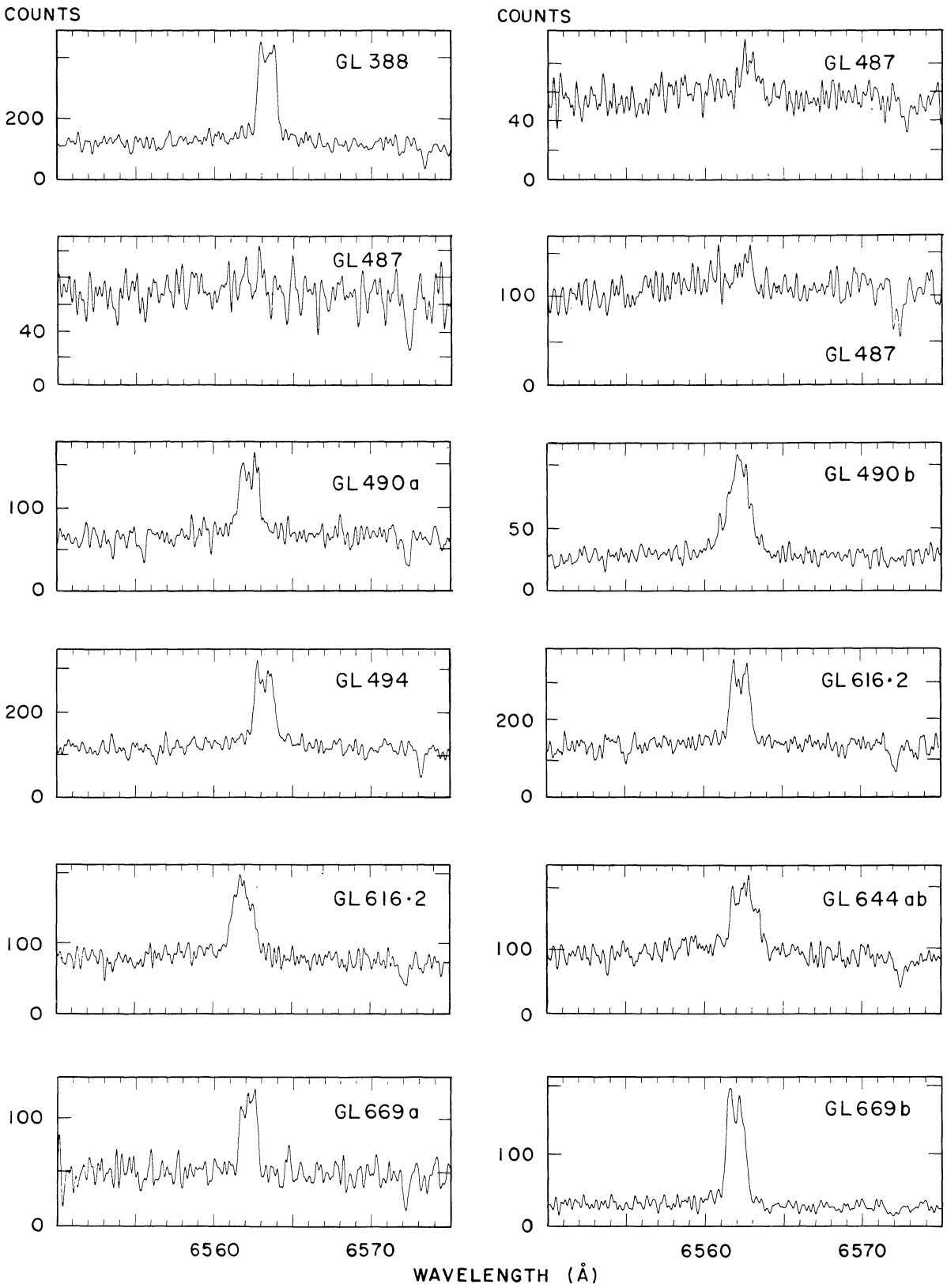

FIG. 2—*Continued*

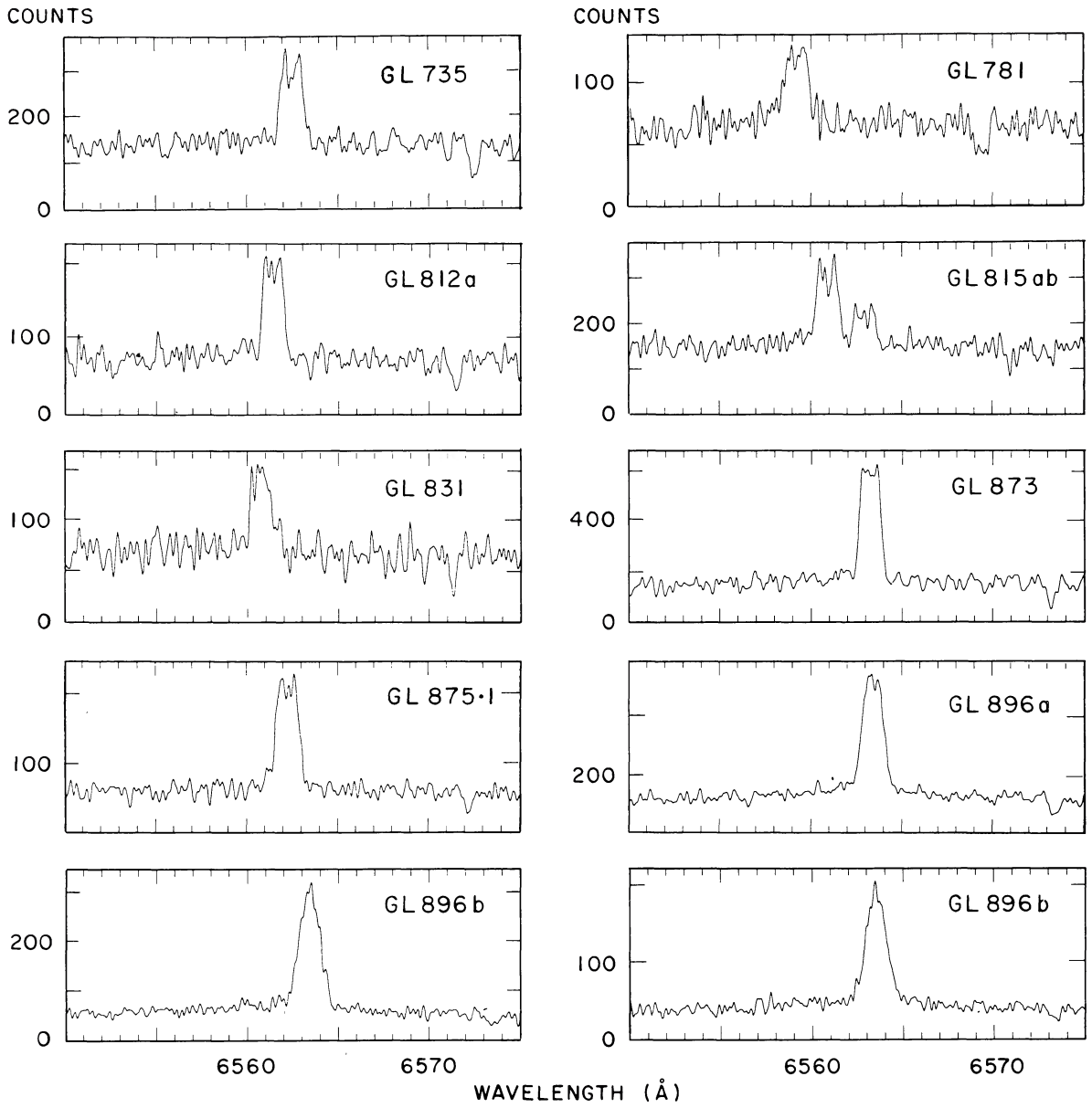

FIG. 2—*Continued*

easily measured with early detectors; for theorists, the calcium lines are favored because they are the most important chromospheric coolants for G and K dwarfs and because interpretation of the observed fluxes in terms of chromospheric cooling is relatively straightforward. Detectors and methods of analyzing spectra have changed considerably in the last two decades, however, and Herbig (1985) has recently shown that high signal-to-noise spectra at Hα can provide some of the same information as the calcium data for G dwarfs. Herbig observed a sample of 40 F8–G3 dwarfs with known chromospheric activity based on Ca II H and K fluxes. By carefully subtracting the spectrum of the least active star from the other spectra, Herbig showed that the cores of the Hα profiles are slightly filled in by emission in the chromospherically active stars. Furthermore, the residual Hα fluxes correlate well with the Ca II H and K fluxes for his program stars. High signal-to-noise observations were required because the maximum residual equivalent width detected by Herbig was about

TABLE 2

GRAVITY-SENSITIVE INDICES FOR THE LOW-DISPERSION SPECTRA

Feature	Interval (Å)	Continuum Regions (Å)
Mg b + Mg H.....	5095–5205	4905–4935, 5285–5315
Na I D	5880–5905	5840–5860, 5860–5877, 5911–5930, 5931–5960
Ca H	6375–6395	6285–6315, 6315–6340, 6396–6430, 6430–6460

TABLE 3

RESULTS OF THE LOW-DISPERSION SPECTROSCOPIC SURVEY

GLIESE	Δ54	TiO59	TiO61	TiO65	Mgb+H	NaID	CaH	$(R-I)_{Tio}$	$(R-I)_{obs}$
GL 4A	-0.046	0.109	0.041	0.172	0.00	7.31	0.00	0.67	0.71
GL 4B	-0.049	0.101	0.041	0.	0.	0.	0.	0.65	
GL 14	-0.060	0.080	0.022	0.	0.	0.	0.	0.60	0.61
GL 15A	0.008	0.161	0.128	0.287	31.24	7.84	2.59	0.86	0.88
GL 15A	0.013	0.164	0.144	0.333	31.37	8.90	3.50	0.89	0.88
GL 15B	0.105	0.	0.	0.	36.46	10.57	0.	1.21	1.26
GL 29.1	0.003	0.146	0.122	0.262	0.	5.85	0.	0.83	
GL 57.1B	-0.020	0.093	0.061	0.147	0.	7.97	0.	0.69	
GL 79	-0.031	0.112	0.067	0.195	31.81	6.96	1.74	0.71	
GL 82	0.132	0.258	0.267	0.613	29.58	8.78	3.32	1.31	1.30
GL 87	0.028	0.160	0.154	0.324	33.37	6.11	2.17	0.91	0.86
GL 105.5	-0.039	0.041	0.000	0.076	37.58	5.70	0.23	0.59	0.65
GL 109	0.072	0.209	0.200	0.449	26.68	6.73	2.65	1.08	1.09
GL 112.1	-0.053	0.041	0.000	0.065	35.16	7.30	0.33	0.57	
GL 114	-0.071	0.041	-0.014	0.042	0.	6.90	0.	0.54	
GL 169	-0.042	0.092	0.047	0.166	36.46	7.59	1.04	0.66	0.62
GL 169.1A	0.124	0.267	0.205	0.515	24.84	6.64	1.66	1.21	1.28
GL 176	0.039	0.180	0.153	0.368	27.72	7.17	2.53	0.95	0.97
GL 182	-0.026	0.099	0.060	0.195	31.50	5.81	0.92	0.70	
GL 184	-0.001	0.135	0.102	0.	0.	0.	0.	0.80	0.76
GL 185A	-0.023	0.099	0.051	0.192	31.99	6.79	1.58	0.70	0.72
GL 205	-0.013	0.196	0.113	0.315	32.02	6.68	1.47	0.87	0.85
GL 205	0.013	0.160	0.121	0.308	29.18	7.31	2.01	0.86	0.85
GL 212	-0.009	0.139	0.086	0.264	27.96	6.07	1.80	0.79	0.81
GL 213	0.134	0.241	0.270	0.579	30.06	6.45	2.57	1.28	1.29
GL 228A	0.070	0.191	0.204	0.429	30.60	5.86	2.25	1.05	1.04
GL 229	-0.002	0.146	0.110	0.283	29.87	7.01	2.01	0.82	0.82
GL 234A	0.190	0.281	0.271	0.583	29.76	7.67	2.75	1.36	1.38
GL 239	-0.021	0.102	0.050	0.190	32.46	7.18	1.96	0.70	0.73
GL 251	0.075	0.214	0.209	0.465	26.28	7.04	2.60	1.10	1.12
GL 273	0.123	0.244	0.219	0.527	26.92	6.78	1.89	1.20	1.22
GL 273	0.110	0.214	0.233	0.514	26.03	6.52	2.44	1.17	1.22
GL 277AB	0.077	0.207	0.174	0.403	24.91	4.80	2.03	1.04	1.08
GL 285	0.145	0.276	0.266	0.575	30.07	7.24	3.02	1.32	1.35
GL 388	0.080	0.183	0.197	0.446	27.99	6.80	2.69	1.06	1.13
GL 388	0.073	0.225	0.210	0.474	30.45	8.14	3.13	1.11	1.13
GL 408	0.043	0.192	0.226	0.439	27.81	7.37	2.91	1.05	1.05
GL 411	0.015	0.195	0.163	0.383	35.20	8.05	2.60	0.95	0.91
GL 447	0.110	0.288	0.241	0.489	29.66	7.93	2.62	1.24	1.35
GL 473AB	0.216	0.307	0.317	0.675	28.38	6.49	3.22	1.50	1.58
GL 486	0.125	0.239	0.248	0.540	27.98	7.49	2.92	1.23	1.23
GL 507B	0.052	0.219	0.216	0.466	30.73	8.31	2.69	1.09	1.08
GL 514	0.009	0.146	0.110	0.296	32.02	8.23	2.46	0.84	0.81
GL 525	-0.024	0.090	0.046	0.169	36.50	7.60	1.39	0.68	0.66
GL 526	0.012	0.162	0.177	0.341	32.93	6.20	1.93	0.92	0.85
GL 526	0.027	0.158	0.155	0.336	31.83	5.10	1.65	0.91	0.85
GL 537	-0.035	0.119	0.052	0.206	20.07	2.47	0.56	0.71	0.83
GL 543	0.080	0.227	0.224	0.488	35.79	8.31	4.27	1.14	1.09
GL 617A	-0.045	0.110	0.057	0.200	35.90	7.54	1.43	0.69	0.68
GL 617B	0.066	0.230	0.202	0.453	29.17	6.50	2.37	1.09	1.08
GL 625	0.025	0.190	0.151	0.387	30.02	6.95	3.03	0.95	0.95
GL 625	0.011	0.193	0.188	0.382	32.71	7.10	2.18	0.97	0.95
GL 630.1A	0.179	0.248	0.284	0.598	38.77	9.33	3.52	1.34	1.32
GL 643	0.121	0.275	0.254	0.564	25.72	8.46	2.66	1.28	1.22
GL 644AB	0.075	0.203	0.214	0.465	32.24	7.05	2.99	1.09	1.08
GL 669A	0.101	0.229	0.213	0.493	29.80	8.37	3.13	1.15	1.21
GL 677AB	-0.064	0.032	-0.007	0.074	34.61	5.13	-0.12	0.55	0.48
GL 697.1	-0.053	0.062	0.025	0.144	35.99	6.83	1.26	0.61	
GL 699	0.117	0.294	0.301	0.581	37.50	10.21	4.00	1.35	1.23
GL 752B	0.371	0.302	0.373	0.767	0.	0.	0.	1.66	
GL 754.1B	0.064	0.231	0.240	0.490	29.22	10.12	3.55	1.14	1.09
GL 812A	0.118	0.283	0.255	0.541	0.	0.	0.	1.28	1.14
GL 815AB	0.018	0.153	0.135	0.330	34.06	6.83	2.74	0.88	0.91
GL 820A	-0.055	0.027	-0.017	0.061	34.16	5.24	0.22	0.55	0.47
GL 820B	-0.039	0.052	0.007	0.116	34.05	6.39	1.13	0.60	0.60
GL 829	0.091	0.219	0.210	0.478	27.25	7.51	2.64	1.12	1.16
GL 830	-0.042	0.060	0.026	0.127	36.78	5.96	0.52	0.62	0.56
GL 830	-0.054	0.055	0.010	0.116	37.34	6.41	0.58	0.59	0.56
GL 846	-0.018	0.163	0.072	0.264	27.85	7.35	1.60	0.79	0.76
GL 846	-0.002	0.125	0.095	0.238	30.97	6.66	1.47	0.78	0.76
GL 851.1	-0.050	0.037	0.003	0.075	34.57	6.97	-.06	0.57	
GL 857.1A	-0.053	0.044	0.004	0.040	0.	0.	0.	0.57	0.54
GL 860A	0.101	0.243	0.230	0.497	27.47	7.80	3.05	1.18	1.15
GL 866	0.257	0.346	0.341	0.725	28.18	4.43	1.93	1.61	1.66
GL 867A	0.025	0.160	0.133	0.350	29.08	6.76	2.47	0.90	0.94
GL 867B	0.087	0.232	0.212	0.505	32.45	6.76	2.90	1.15	1.20
GL 873	0.091	0.231	0.236	0.500	0.	0.	0.	1.17	1.20
GL 873	0.094	0.259	0.224	0.522	26.67	7.17	3.63	1.20	1.20
GL 880	0.022	0.192	0.125	0.332	26.39	7.79	2.08	0.91	0.88
GL 880	0.001	0.173	0.116	0.265	0.	0.	0.	0.85	0.88
GL 884	-0.022	0.091	0.072	0.154	28.87	4.20	0.15	0.70	0.62
GL 896A	0.086	0.224	0.232	0.497	30.76	6.95	3.00	1.15	1.13

0.1 Å, as compared with a typical Hα absorption equivalent width of 4 Å for a solar-type star.

As noted by Fosbury (1974), Cram and Mullan (1979, hereafter CM) and Giampapa (1985), Hα becomes a more attractive chromospheric index for M dwarfs. The photosphere of an M dwarf is expected to produce only a very weak Hα absorption line because it is too cool to populate the $n = 2$ level of hydrogen significantly; Mould's (1976*a*) model M dwarf with $T_{\rm eff} = 3500$ K (spectral type about M2, $R - I \approx 0.9$ according to the calibration of Mould and Hyland 1976) has a predicted photospheric Hα absorption equivalent width of 0.08 Å. By contrast, the chromosphere of an M dwarf can produce a strong Hα line, which will either be in emission or in absorption depending on the photospheric radiation temperature, the electron density at the base of the chromosphere, and the temperature gradient in the chromosphere. For an M dwarf with $T_{\rm eff} = 3500$ K, CM's model calculations, which assume a two-stage temperature gradient in the chromosphere linear with the log of the mass column density, predict a maximum total Hα absorption of −0.7 Å for $\log N_e = 10.6$ at $T(\text{chrom}) = 9000$ K, with Hα becoming an emission feature for higher values of $N_e(9000)$ or cooler photospheric temperatures. The expected dependence of Hα equivalent width on $N_e(9000)$ is provided by CM in their Table 1. Giampapa (1985) notes that for a very late M dwarf the photospheric radiation field should be so weak that Hα will be collisionally dominated for all chromospheric electron densities. In that event, chromospheric Hα absorption is not possible; either Hα will appear in emission, or no Hα feature will be present at all.

Complications for this relatively simple picture have been noted by Young, Skumanich, and Harlan (1984) and Giampapa (1985). The primary difficulty with the use of Hα as a chromospheric indicator for M dwarfs is the inability to establish a one-to-one relation between Hα equivalent width and chromospheric activity. That is, for dM stars with relatively weak Hα absorption, the possible explanations include (1) a relatively thin chromosphere; (2) a relatively thick chromosphere, but with electron density in the transition region between maximum Hα absorption and Hα emission; or (3) a composite (inhomogeneous) chromosphere, with regions of both Hα absorption and Hα emission. Interpretation of the Hα equivalent widths therefore requires discrimination between these various possibilities. One star in our sample, GL 410, has been previously identified as having a composite chromosphere by Young, Skumanich, and Harlan (1984). That conclusion was based on photometric evidence obtained by Bopp *et al.* (1983) indicating that GL 410 is a short-period, BY Draconis variable.

We have insufficient information for our M dwarf sample to completely resolve the ambiguity in the interpretation of the Hα equivalent widths for all of our program stars. Instead, we will use the broad-band photometry provided in Table 1 to sort the stars into several groups with different mean chromospheric activity levels. Is Hα a viable activity index for M dwarfs? To what extent do Hα lines emitted by real stars match the models published by Mould (1976*a*) and CM? Do M dwarfs without measurable chromospheres exist?

a) Distribution of Hα *Equivalent Width in the* (Hα, $R - I$)*-Plane*

Both the strength of the photospheric Hα absorption line and the formation of Hα in the chromosphere should vary strongly with spectral type among the M dwarfs. We therefore need to choose an indicator of spectral type or effective temperature as the independent variable for our examination of the Hα equivalent width data. We have selected ($R - I$) as measured in the Kron system (KGW; Eggen 1975) both because of the availability of ($R - I$) photometry and because ($R - I$) has been shown to be a good temperature index for M dwarfs (Mould and Hyland 1976). For many of the stars we have ($R - I$) photometry of our own; for the rest we have used ($R - I$) data from Gliese (1969*a*) and Eggen (1979, 1980). In order to preserve homogeneity, the only Hα data we will use are our own.

A plot of Hα equivalent width versus ($R - I$) for all of our program stars is shown in Figure 3. The majority of the stars have Hα in absorption. Our data confirm the well-known result (Petit 1961; Joy and Abt 1974) that the fraction of stars with Hα in emission increases for redder stars. The mean Hα equivalent width for the dMe stars increases toward later spectral types also, but this reflects primarily the decreasing photospheric luminosity and not an increase in chromospheric activity. The average surface flux in Hα emission from the stars in our dMe sample does not vary significantly with $R - I$. We note, however, that spottedness may increase toward later spectral types—10 of the 15 stars listed as photometric variables in § II have $R - I > 1.1$.

A more informative representation of our Hα data is shown in Figure 4, where we have excluded most of the dMe

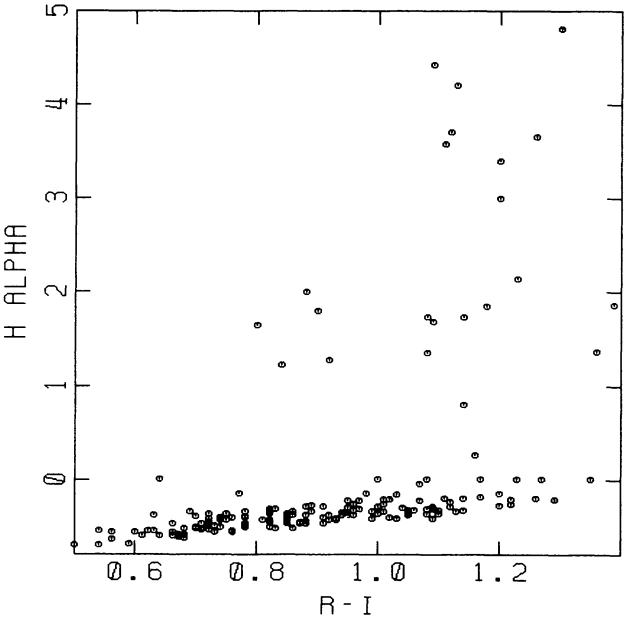

FIG. 3.—Mean Hα equivalent width vs. $R - I$ for the stars in Table 1. Negative values correspond to Hα in absorption, positive values to Hα emission. Spectral type and color equivalents are M0, $R - I = 0.60$; M2, $R - I = 0.80$; M4, $R - I = 1.10$; and M5, $R - I = 1.25$.

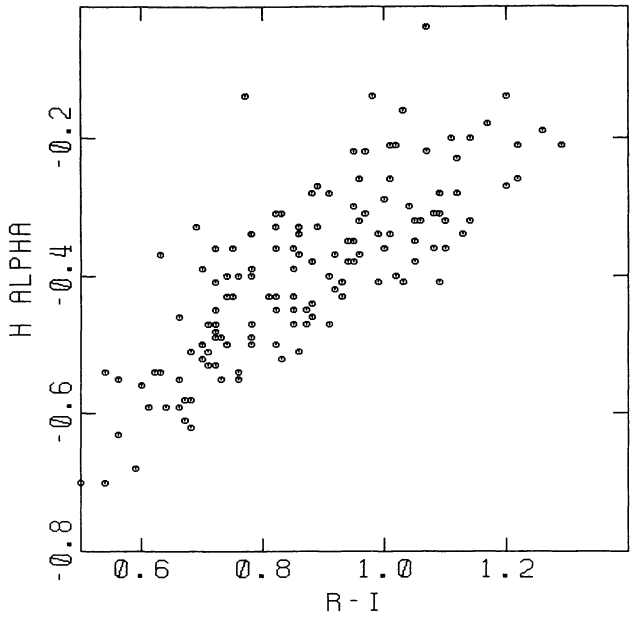

FIG. 4.—Mean Hα equivalent width vs. $R - I$ for only the stars with Hα in absorption.

stars from the plot. Several interesting facets of the data are discernible in this figure.

1. A number of the stars, generally with quite red colors, have no detectable feature at Hα. Two examples are shown in Figure 5.

2. The mean Hα absorption equivalent width becomes weaker toward redder $(R - I)$ colors, as expected on the basis of the discussion by CM.

3. There appears to be a spread in Hα absorption equivalent width at fixed $(R - I)$ that is larger than our measuring error.

We will discuss this last point at some length, since it provides the basis for most of our conclusions. Our evidence for this statement can be illustrated in two ways. First, as we have previously discussed in § II, consideration of the signal-to-noise ratio in our spectra or comparison of multiple spectra of the same star indicates that our equivalent widths are generally accurate to about 0.03 Å. The observed spread in equivalent width at a given $(R - I)$ is many times larger. As a second argument, we show in Figure 6 the spectra of several stars with nearly the same $(R - I)$, but for which we list quite different Hα equivalent widths. The strong metal line redward of Hα is approximately the same strength in each star, while the Hα line shows an obvious variation.

Within the context of the CM models, the spread in Hα equivalent width at fixed $(R - I)$ shown in Figure 4 could be interpreted in several ways. Those stars with the strongest Hα absorption must have relatively dense chromospheres, since at $R - I = 0.90$ the predicted photospheric Hα absorption equivalent width is only 0.08 Å, and our maximum observed equivalent width is 0.50 Å. However, as discussed previously, without further information it is not possible unambiguously to assign any particular chromospheric activity level to stars with relatively weak Hα absorption.

b) Separating the Sheep from the Goats

As a first step in identifying the causes for the spread in Hα equivalent width shown in Figure 4, it is useful to attempt to locate a subset of stars that would be expected to have weak chromospheric activity. We have chosen a set of presumed

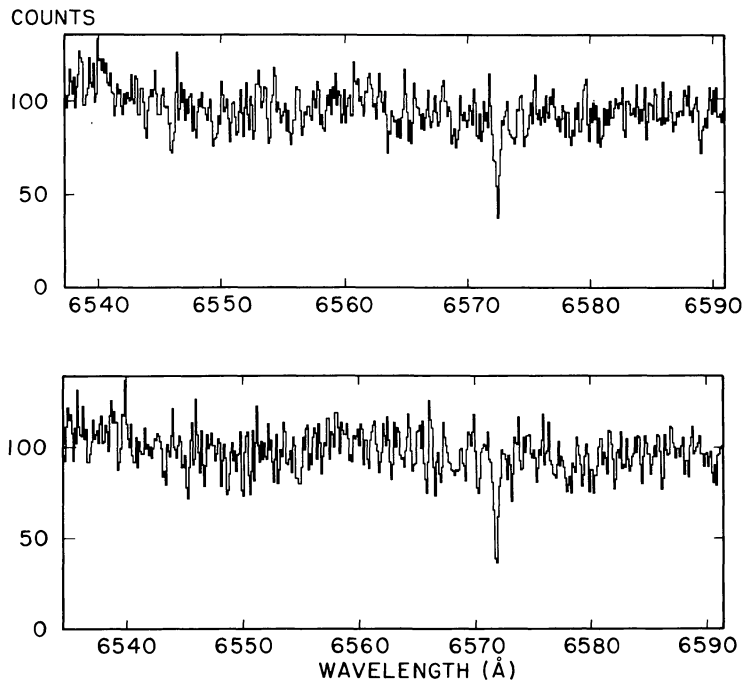

FIG. 5.—Sample spectra for two dM stars with approximately continuous spectra at Hα. Possible very weak Hα absorption or emission features are sometimes present in the spectra of both stars.

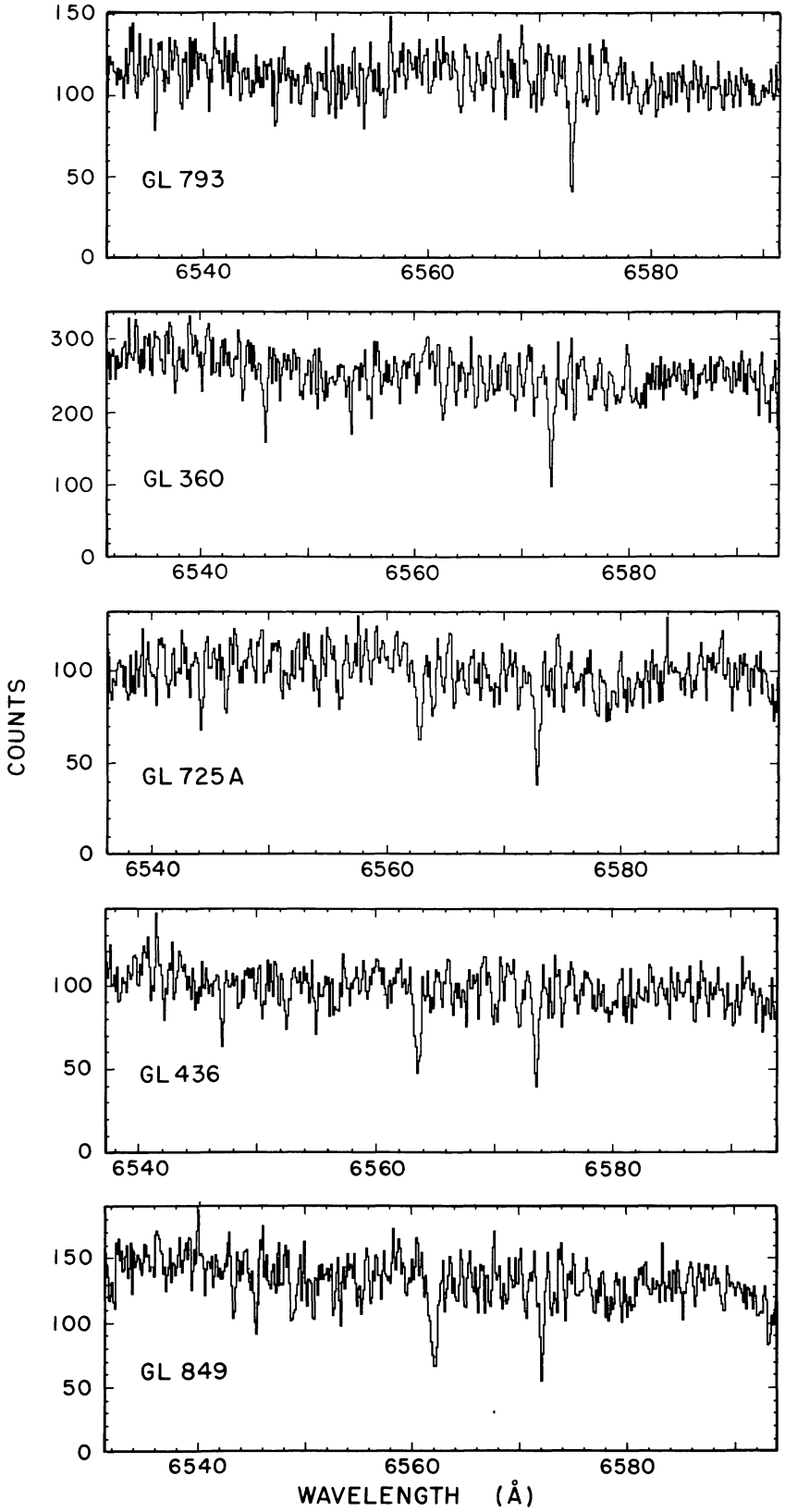

FIG. 6.—Spectra in the vicinity of Hα for five stars with $R - I \approx 1.05$, but with greatly varying Hα absorption equivalent widths. Note that the Ca I feature at $\lambda \approx 6572$ remains approximately constant in strength for each star.

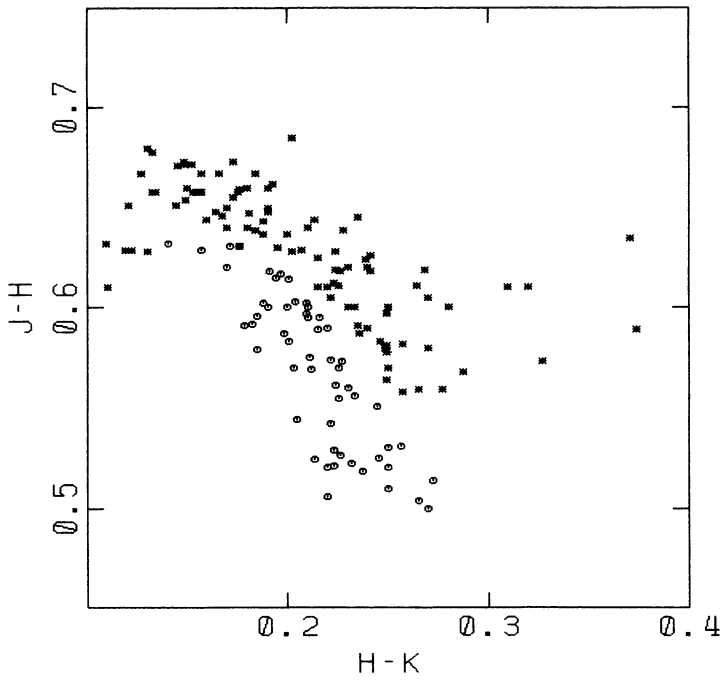

FIG. 7.—Infrared color-color diagram in the CIT system for the M dwarfs in Table 1. Stars with approximately solar metallicity are shown as asterisks. Stars shown as open circles occupy a region believed to be populated by metal-poor stars according to Mould and Hyland (1976).

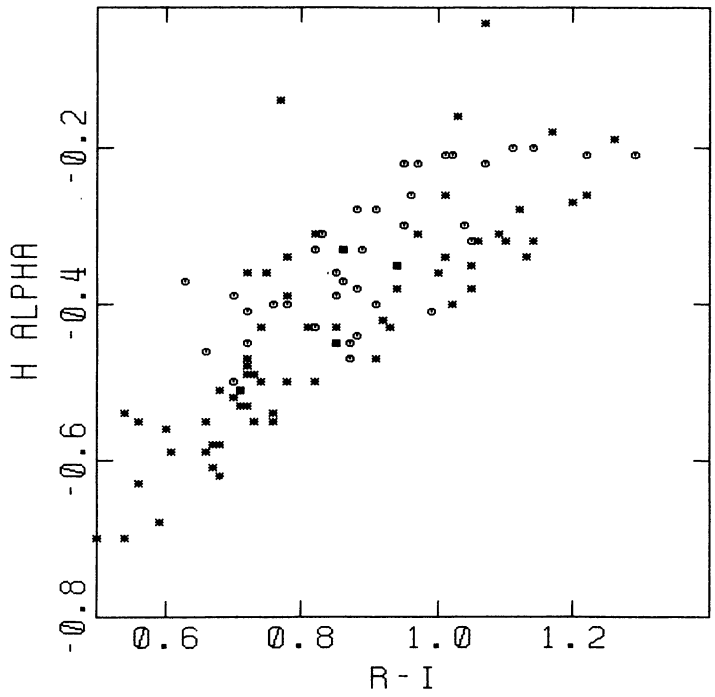

FIG. 8.—Equivalent width of Hα vs. $R - I$ for the primary sample, with symbols as identified in Fig. 7. Only stars with *JHK* photometry are plotted.

metal-poor M dwarfs to make this test. The underlying assumptions are (1) that metallicity and age are well correlated, so that metal-poor stars are, on average, old; (2) that old stars have, on average, weaker chromospheres than young stars; and (3) that within the metallicity range we expect to encounter, any intrinsic dependence of the photospheric or chromospheric Hα equivalent widths on metallicity is negligible. With respect to the last point, Mould (1985) expects no significant metallicity dependence for the photospheric Hα absorption line, and Cram and Mullan's model calculations suggest that for two otherwise similar chromospheres, the more metal-poor model will have stronger Hα absorption. A metallicity dependence of that sign will only strengthen our conclusions.

We employ an infrared two-color diagram to select the candidate metal-poor stars. Using data from Table 1, supplemented by photometry for a few stars from Persson, Aaronson, and Frogel (1983, hereafter PAF), we have produced the $(J-H, H-K)$-diagram for our program stars shown in Figure 7. The separation of the diagram into regions of low and "normal" metallicity follows the work of Mould and Hyland (1976) and of PAF. Those authors showed that metal-poor stars are blue in $J-H$ for a given $H-K$ color relative to metal-rich stars. The explanation for this effect, which stems from the fact that H^- has its opacity minimum at about 1.6 μm (the center of the H band), can be found in Mould (1976*a*). Observational verification that the stars that are blue in $J-H$ are metal-poor is provided in Mould (1976*b*) and Mould and Hyland (1976), as well as in § IV of this paper, where we show that these stars tend to be subdwarfs in an $(M_V, R-I)$-diagram and have high surface gravities.

By assumption, the metal-poor stars identified in the infrared two-color diagram should have weak chromospheres. In Figure 8 we replot the (Hα, $R-I$)-diagram with different symbols for the metal-poor and normal metal samples (*asterisks*: normal metallicity; *open circles*: metal-poor; stars without infrared data are not plotted). Most of the metal-poor stars do have relatively weak Hα absorption for their $(R-I)$ color. We view this as strong confirmation that chromospheres can be a dominant contributor to the Hα absorption line in M dwarfs and that the initial response to increased chromospheric activity is to produce a stronger Hα absorption line.

A significant number of the Hα weak stars in Figure 8 do not have colors corresponding to the metal-poor region of the $(J-H, H-K)$-diagram. These stars could simply be metal-rich but chromospherically weak stars, or they could correspond to any of the previously described active chromosphere scenarios. One of the stars in this group is GL 410 (Hα = -0.14, $R-I=0.77$), which almost certainly has an active chromosphere because it is a short-period, BY Draconis variable (Bopp *et al.* 1983).

We suspect that most of the remaining weak Hα, normal *JHK* stars are also chromospherically active, based on an examination of their kinematics. Space motions in the (U, V, W)-plane have been calculated for our program stars using the apparent magnitudes listed in Table 1 or in Gliese (1969*a*) or Eggen (1979, 1980); radial velocities from our survey; proper motions from Gliese; and trigonometric parallaxes from van Altena (1985). The space motions are corrected to the local standard of rest, using the solar motion from Woolley *et al.* (1970). In Figures 9 and 10 we show the (U, V)- and (V, W)-diagrams for four sets of stars: (1) the metal-poor, weak Hα stars just identified; (2) the normal metallicity, weak Hα stars; (3) stars with normal metallicity judged by the $(J-H, H-K)$-diagram and strong Hα absorption; and (4) stars with Hα in emission. Weak and strong Hα absorption are defined arbitrarily relative to the lower envelope to the (Hα, $R-I$) distribution shown in Figure 4, given by H$\alpha = 0.62(R-I) - 1.028$. Stars with H$\alpha$ equivalent widths within 0.1 Å of this relation are considered Hα-strong; those with Hα equivalent widths more than 0.1 Å weaker (but not in emission) are considered to be weak Hα absorption stars. A summary of the kinematic data is provided in Table 4. The dMe stars show the well-known result of having small space motions typical of young disk objects, with the notable exception of GL 781 ($U=25$, $V=178$, $W=-79$). It is somewhat surprising that there is so little difference between the metal-poor sample and the normal metal, strong Hα stars in the two figures, since we expect the former group to be older. The most obvious facet of the two figures, however, is the close similarity in motions between the dMe stars and the normal metal, weak Hα stars. We conclude from this that the latter group is indeed young, and hence that their weak Hα absorption is evidence that they are active chromosphere stars, just slightly less active than the dMe's.

Table 5 provides a list of the normal metallicity, weak Hα stars that we have identified as chromospherically active. In the table we provide the star's $R-I$ color, the displacement of the Hα equivalent width from the lower envelope to the (Hα, $R-I$) distribution, the displacement of the star relative to a provisional main-sequence $(M_V, R-I)$-relation, and a Ca II S index for the star when available, from the survey of Vaughan and Preston (1980), kindly made available by Dr. Vaughan. The Ca II data serve as additional confirmation that the stars in Table 5 are chromospherically active. The mean Ca II S index for the weak Hα, normal metallicity sample is slightly more than twice as great as for the weak Hα, metal-poor set of stars. The absolute magnitude displacements serve primarily as a consistency check in this case, since the selection by *JHK* colors ensures that the weak Hα, normal metallicity sample of stars will be approximately on the solar-metallicity main sequence, while the weak Hα, metal-poor sample will be displaced below the main sequence.

A significant fraction of the stars observed spectroscopically have been excluded from the preceding discussion because no infrared photometry is yet available. To search among this group for other possible weak Hα, chromospherically active stars, we have used the secondary criteria of displacement above the $(M_V, R-I)$ main sequence, Ca II emission strength, and the strength and variability of the Hα equivalent width. The best candidates from this group are GL 900, which is the bluest star (by 0.35 mag in $R-I$) in our sample with an essentially continuous spectrum at Hα. The Hα region in GL 900 may be variable, since one of our spectra appears to show a very weak Hα emission feature. The other good active chromosphere candidate is GL 49,

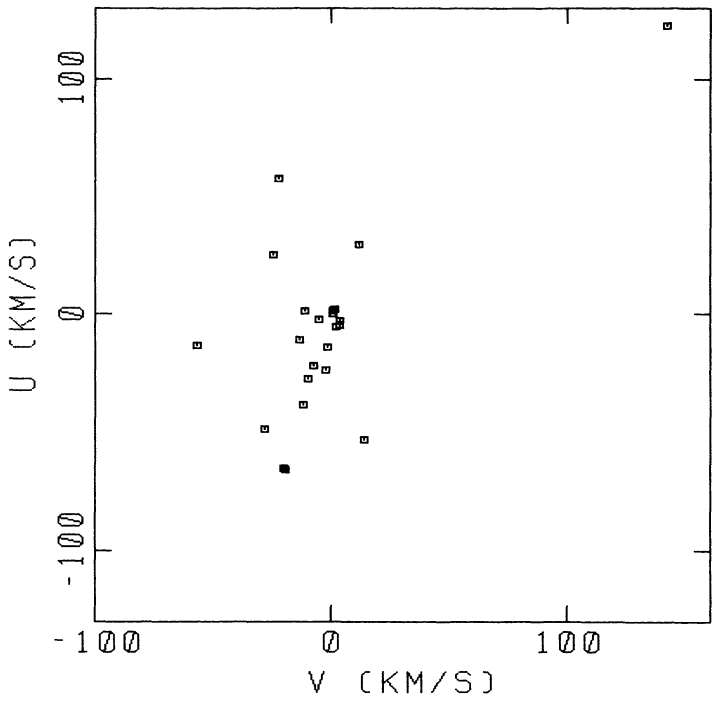

FIG. 9*a*

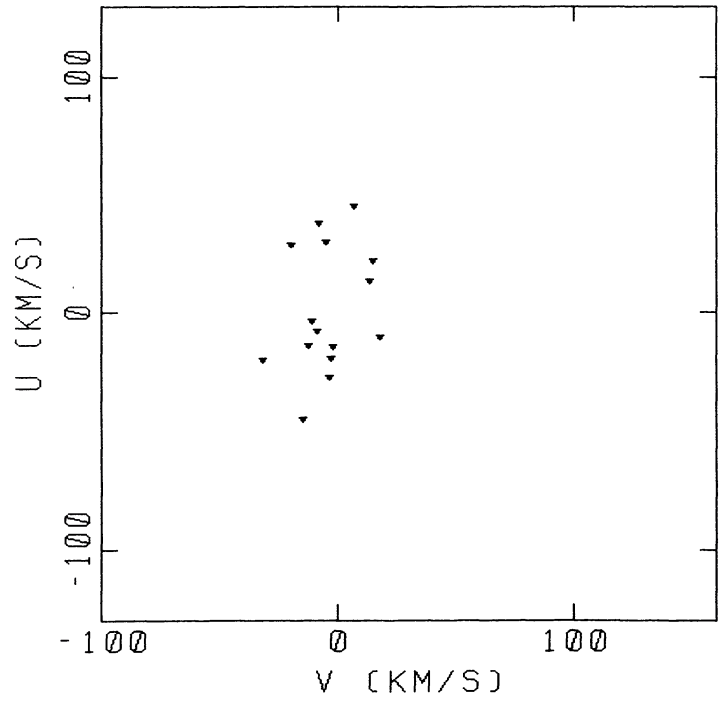

FIG. 9*b*

FIG. 9.—Space motions in the (U, V)-plane for four sets of stars ordered by chromospheric activity. Panels $a-d$ correspond, in order, to the dMe stars; the weak Hα absorption, normal metallicity stars; the strong Hα absorption set; and the weak Hα absorption, metal-poor group.

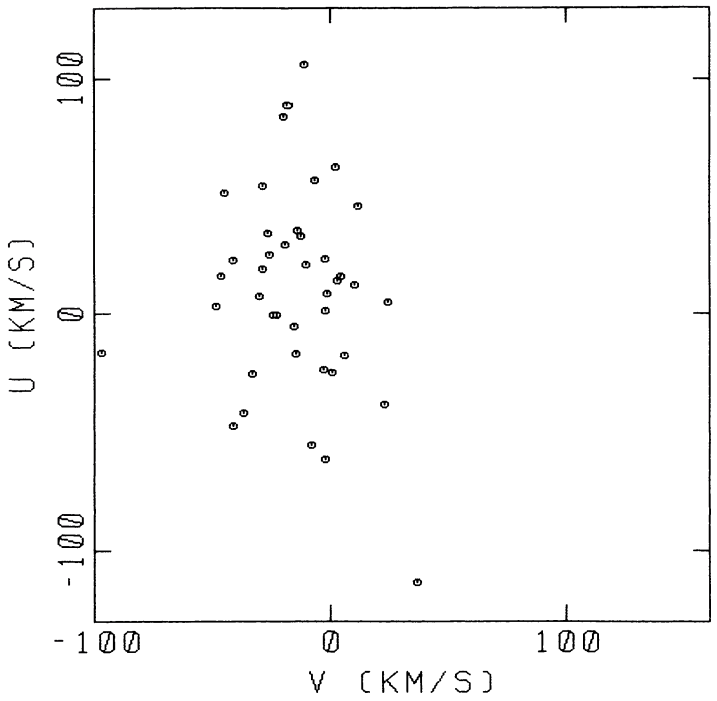

FIG. 9*c*

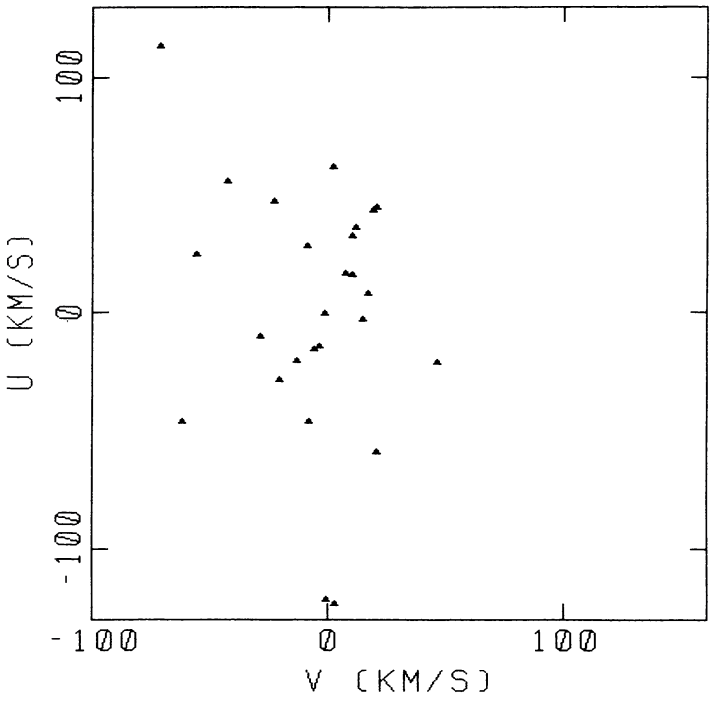

FIG. 9*d*

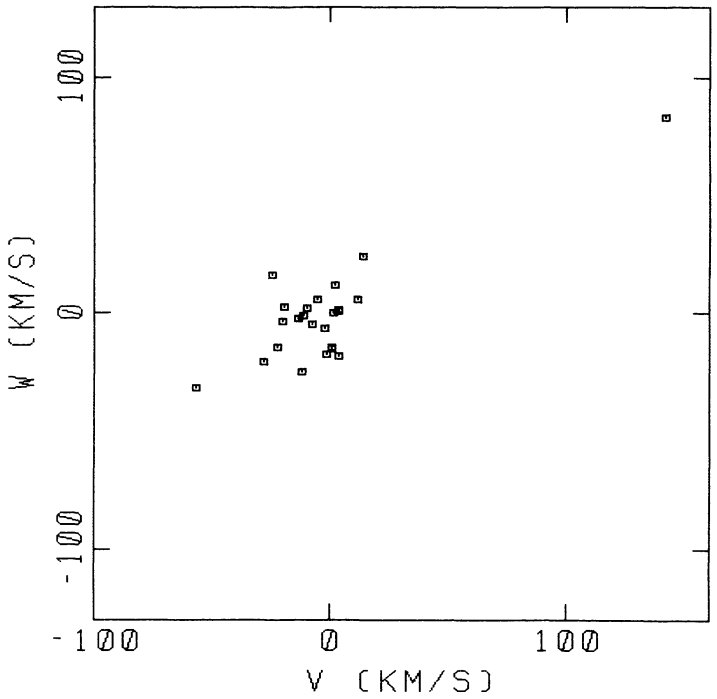

FIG. 10*a*

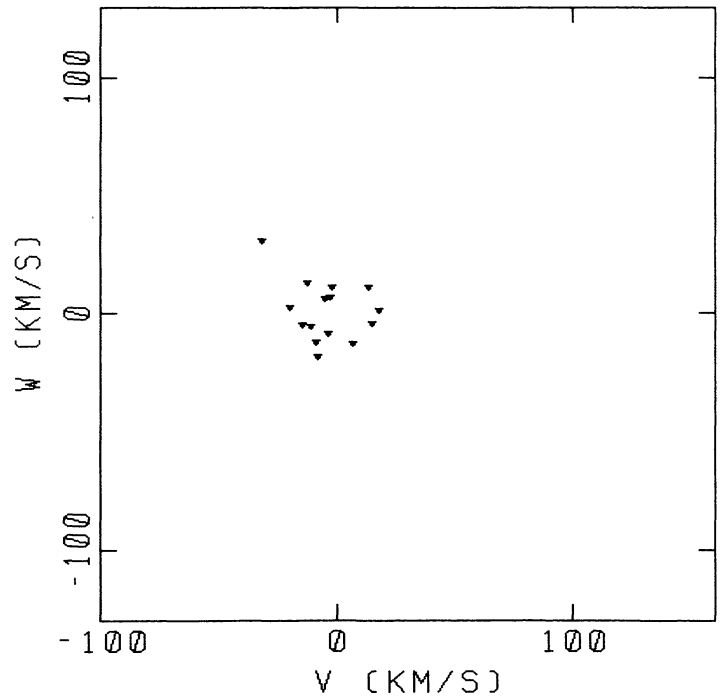

FIG. 10*b*

FIG. 10.—Space motions in the (V,W)-plane for samples of differing chromospheric activity. The arrangement of the panels is the same as for Fig. 9.

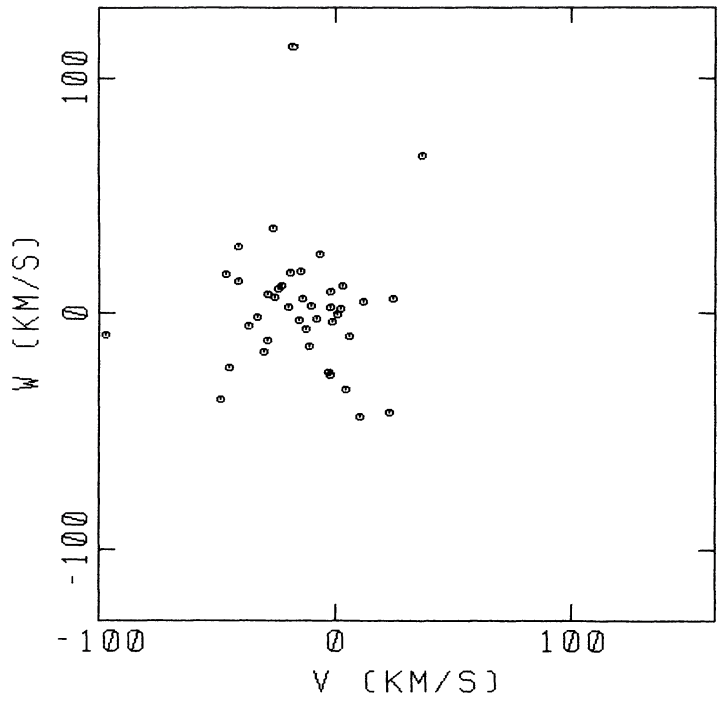

FIG. 10*c*

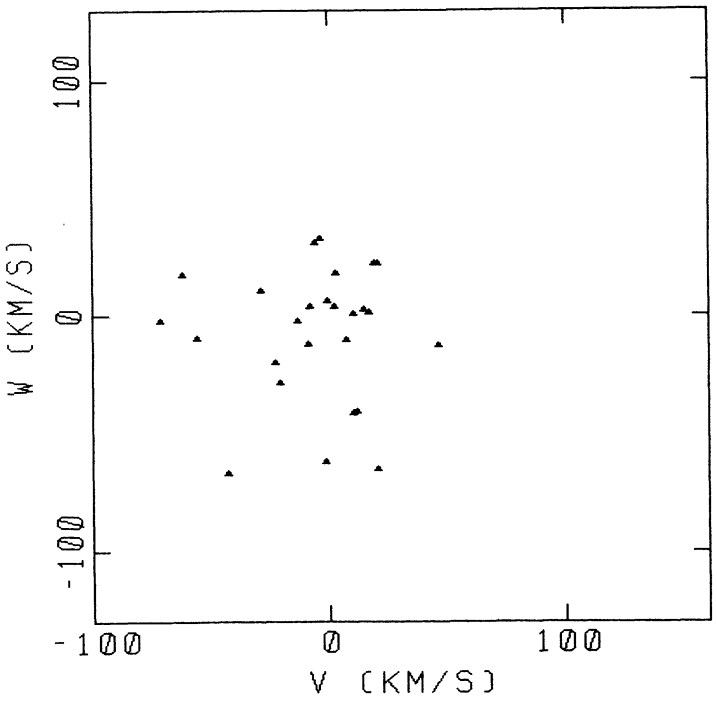

FIG. 10*d*

TABLE 4

KINEMATICAL DATA FOR M DWARF SUBSETS

Sample	N	$\langle U \rangle$	$\langle V \rangle$	$\langle W \rangle$	σ_U	σ_V	σ_W
dMe	23	−12.4	−8.5	−4.5	28.7	15.1	13.2
Active, weak Hα	14	1.1	−4.7	1.2	25.9	12.9	12.1
Active, strong Hα	42	10.3	−14.5	2.8	42.1	23.5	26.9
Inactive, weak Hα	26	0.7	−6.3	−7.7	52	27.2	27.7

NOTE.—The results for the dMe stars have been derived after exclusion of GL 781 from the sample. Velocities are in km s^{-1}, corrected to the local standard of rest.

TABLE 5

NORMAL METALLICITY STARS WITH WEAK Hα ABSORPTION

Star	U	V	W	ΔHα	ΔM_V[b]	Ca II
Likely Candidates						
GL 49	−14.1	−12.4	13.1	0.21	0.28	2.39
GL 212	−3.2	−11.1	−5.3	0.21	0.16	2.20
GL 360	−27.1	−4.2	−8.5	0.23	0.82	...
GL 410	22.3	14.5	−3.8	0.41	−0.08	...
GL 458.2	−7.8	−9.1	−12.1	0.22	0.16	...
GL 649	30.0	−5.0	6.5	0.16	0.03	1.91
GL 685	45.3	6.7	−12.9	0.15	0.22	...
GL 694.2	13.5	12.7	11.2	0.20	0.51	2.35
GL 730	28.7	−20.1	2.6	0.15	−0.15	1.74
GL 793	−9.9	17.4	1.3	0.32	0.02	1.97
GL 804	38.4	−8.4	−18.3	0.14	−0.19	1.61
GL 844	−19.4	−3.1	7.0	0.14	0.63	...
GL 851	−19.8	−31.5	30.5	0.12	0.40	1.80
GL 900	−14.7	−2.5	11.0	0.64	0.22	...
Less Likely Candidates						
GL 176	−32	−30	−55	0.11	0.40	...
GL 469	−14	−19	−13	0.14	0.13	...
GL 471	−7	−47	+9	0.11	0.33	2.02
GL 516A	37	10	−3	0.42	−0.24	1.92
GL 516B[a]	37	10	−3	...	...	1.26
GL 829	−28	−7	3	0.12	0.31	...
GL 875	11	14	19	0.12	0.03	...
GL 895	−4	−34	−4	0.15	0.56	...

[a] No $R-I$.

[b] Positive values indicate displacement above the ZAMS.

which is 0.3 mag brighter for its color than the standard main-sequence relation and has strong Ca II emission. Because we believe that these stars are quite likely to be active, we included them in the original list of weak Hα, normal metallicity stars given at the top of Table 5. At the bottom of Table 5 we list a few more stars chosen from the group without infrared data which we believe are possible, but less likely, active chromosphere stars. One of the stars at the bottom of the table, GL 176, has a quite large W velocity, which would seem to make it unlikely to be a member of the young disk population. We include it in the sample because it was listed by Joy and Abt (1974) as a dMe and because it is a photometric variable according to Bopp and Espenak (1977). If the Joy and Abt classification was not due to some type of error, GL 176 had an active chromosphere at one time, making it more likely that the weak Hα absorption line we observe is also due to an active chromosphere.

c) *Stars with No Detectable Feature at* Hα

A small number of stars in our sample appear to have continuous spectra in the region where Hα is expected. We have arbitrarily listed their Hα equivalent widths in Table 1 as 0.01 Å. It is possible that higher signal-to-noise spectra would allow identification and measurement of a real feature. Any attempt to measure an equivalent width for Hα in these stars with our spectra would be dominated by noise spikes and the choice of a continuum level. Examples of the spectra of two of these stars are shown in Figure 5.

The possible causes for the lack of Hα in the spectra of these stars are essentially the same as those considered to explain the weak, but detected, Hα absorption-line stars discussed in the preceding section. However, stars with observed Hα equivalent width ~ 0.0 that are early enough for their photospheric Hα absorption line to be stronger than our detection limit (about 0.05 Å) must have their Hα absorption line filled in by some process. Therefore, to the extent that Mould's model calculations are considered accurate in predicting photospheric Hα absorption, stars with no detectable Hα bluer than about $R-I=1.0$ must have active chromospheres. One star, GL 900, with $R-I=0.63$, obviously falls in this category; GL 516A, with $R-I=1.00$, is a possible candidate. Three of the stars, GL 105B, GL 447, and GL 568AB, are of sufficiently late type that an explanation assuming essentially no photospheric or chromospheric Hα features may be viable (Giampapa 1985).

In Table 6 we provide a list of the properties of this set of stars. The table does not provide an unambiguous explanation for the spectroscopic results. That is, GL 900 is the only star with a well-defined pedigree. Two of the stars, GL 507B and GL 516A, have quite strong Ca II emission and are relatively blue, making them seem likely active chromosphere stars. Furthermore, GL 516A is listed in Joy and Abt (1974) as a dMe and is the flare star VW Com. Because it is displaced somewhat below the standard main-sequence relation, we have included GL 516A (and GL 516B) only among the possible active chromosphere stars in Table 5. The second star, GL 507B, is more of a quandary, because it is displaced below the standard main sequence by 1.2 mag. Upgren and Weis (1975) and Hartwick, Crampton, and Cowley (1976) considered GL 507B to be a subdwarf. The best classification of GL 507B is probably that it is the slightly less active counterpart of the dMe stars with old disk motions, such as GL 15B and GL 781.

TABLE 6

STARS WITH NO DETECTABLE FEATURE AT Hα

Star	$R-I$	U	V	W	ΔM_V	Ca II
GL 105B	1.27	−70.6	10.2	44.0	−0.06	...
GL 447	1.35	28.2	15.5	−25.8	...	...
GL 507B	1.08	44.1	−8.5	0.1	−1.23	2.87
GL 516A	1.00	37.2	10.2	−2.7	−0.24	1.92
GL 516B	...	37.4	10.2	−2.0	...	1.26
GL 568AB	1.23	−32.4	−16.1	−11.4	0.32	...
GL 597	1.12	94.4	6.3	−26.3	−0.35	...
GL 860AB	1.17	34.2	−19.0	9.1	−0.10	...
GL 900	0.63	−14.7	−2.5	11.0	0.22	...

d) Comparisons of the Hα Data with Theory

The only published theoretical model which predicts quantitative Hα equivalent widths for realistic M dwarfs is that by CM. As previously noted, for their specific model for a star with $T_{\rm eff} = 3500$ K, they determined a maximum Hα absorption equivalent width of -0.69 Å. The photospheric contribution to the Hα equivalent width was -0.08 Å, as adopted from Mould's (1976*a*) model. Less dense chromospheres than the maximal model produced weaker Hα absorption because of the decreased optical depth, while increasing the density of the chromosphere begins to shift the Hα line from radiation-dominated to collisionally dominated and thus fills in the absorption line with emission.

One possible interpretation of our Hα equivalent width data has already been discussed by Giampapa (1985). In order to derive a lower limit to the fraction of a dM star's surface covered by a chromosphere, Giampapa assumed a two-component model—dense chromospheric regions with maximal Hα absorption and other regions with chromospheres sufficiently thin to produce a negligible Hα feature. A star covered by an equal fraction of the two chromospheric regions would then have an integral Hα equivalent width of -0.35 Å at $R - I = 0.9$ if the CM model applies. By consulting a preliminary version of Figure 4 of this paper, Giampapa determined the minimum and maximum Hα equivalent widths for stars near $R - I = 0.9$, from which he derived an estimated range of minimum active chromosphere covering factors of 0.31–0.67 for these stars.

Even within the general context of the CM model, Giampapa's minimum areal coverage model is only one possible interpretation of the Hα equivalent width data. An alternative, and equally extreme, model would be that all of the dM stars have homogeneous chromospheres, and that the spread in equivalent widths simply reflects a spread in chromospheric mass column densities. In this context, the range in equivalent widths at $R - I \approx 0.9$ from EW(Hα) $= -0.22$ for the presumably old, metal-poor GL 745A to EW(Hα) $= 2.00$ for GL 494 would imply a range in electron densities at the base of the chromosphere from $\log N_e \approx 9.4$ to $\log N_e \approx 11.4$.

Both of the preceding interpretations of the spread in Hα equivalent width appear to conflict with at least one portion of the CM model. Either for areal filling factors greater than 0.67 in the inhomogeneous model, or for electron densities $9.6 < \log N_e < 10.7$ in the homogeneous model, Hα equivalent widths between -0.5 and -0.7 are predicted. But none of the program stars with $R - I \approx 0.9$ have Hα equivalent widths in that range. Since stars with weak Hα absorption and with Hα emission are observed, there is no reason why this intermediate region of parameter space should be avoided. One possible explanation is that the CM model is inaccurate in predicting the maximum Hα absorption, and that the correct value corresponds to our maximum observed Hα equivalent width [EW(Hα) $= -0.50$ at $R - I \approx 0.9$]. In support of this hypothesis, we note that what really controls the formation of Hα is not $T_{\rm eff}$ but is instead the radiation temperature of the Balmer continuum. CM assume that T(Balmer) is equal to $T_{\rm eff}$, whereas blanketing effects in dM stars in reality cause T(Balmer) to be less than $T_{\rm eff}$. The sign of this effect causes the CM model for $T = 3500$ K actually to apply more closely to a star with larger $T_{\rm eff}$. We suspect that this may explain much of the difference between CM's predicted maximum Hα absorption and what we observe at $R - I = 0.90$.

By analogy with the Sun and the other young, late-type stars observed by Wilson (1978), the chromospheres of many of the M dwarfs in our sample are not likely to be homogeneous. Large, inhomogeneously distributed starspots are known to exist on a number of our program stars (from the photometric variability), and many of the rest are likely to be affected by smaller scale starspots. Since we observe some stars with Hα in emission, there must be a significant incidence of regions dense enough to produce Balmer emission lines. Assuming that the chromospheres of such mottled stars can be represented by a combination of regions of differing activity, our observed Hα equivalent width distribution would reflect that dispersion. For stars with inhomogeneous chromospheres, the maximum observed Hα absorption at $R - I = 0.90$ would necessarily be driven to smaller absolute values than predicted by CM, since a portion of the star would now be covered by regions with electron densities either smaller than or greater than that needed to produce maximum Hα absorption. For example, if the electron densities at the base of the chromosphere were distributed as a Gaussian in the log of the electron density, a dispersion of 0.5 in the mean log electron density would decrease the maximum observed absorption equivalent width from -0.69 to -0.53 Å. We do not advocate this specific density distribution, but merely note that assuming a mixture of quiescent surface, spots, and plages would naturally bring the maximum Hα absorption of the model star closer to our observational result.

What does the distribution of Hα equivalent widths imply about the evolution of chromospheric activity among nearby M dwarfs? For other chromospheric activity indices and other spectral type ranges, it is usually assumed that an increase in index strength corresponds to a stronger chromosphere. At least for the CM model M dwarfs, that is not the case for Hα, since an increase in chromospheric column density may cause either stronger Hα absorption or stronger Hα emission. Therefore, interpretation of the distribution of Hα equivalent widths at $R - I = 0.90$, where only about one in 10 stars has Hα in emission, would require considerable faith in the quantitative accuracy of the CM model. For redder colors, however, the fraction of stars with Hα in emission increases, making it possible to use the Hα distribution without recourse to the CM model. In particular, for $R - I > 1.05$, approximately one-third of our sample has Hα in emission. We can use the distribution of Hα equivalent widths for $R - I > 1.05$ to determine an *e*-folding time scale for chromospheric decay in late M dwarfs assuming that (1) the Pleiades Hα equivalent widths (Fig. 23) can be used to normalize the theoretical distribution at $t = 7 \times 10^7$ years; (2) the star formation rate has been constant throughout the approximately 10×10^9 year lifetime of the disk; and (3) our sample of stars is unbiased. The latter two assumptions are invalid to varying degrees, but are good enough for our limited purposes. Given these assumptions, we derive an Hα *e*-folding time scale of $\tau \approx 1.2 \times 10^9$ years for late-type M dwarfs, obviously with large error bars. This is shorter than the *e*-folding time scale

found for Hα by Herbig (1985) for G dwarfs, but comparable to time scales for other chromospheric emission lines observed by Simon, Herbig, and Boesgaard (1985).

An alternative and simpler method of describing the evolution of Hα activity for M dwarfs is to estimate the time needed for the chromosphere to decay sufficiently for Hα to become an absorption feature. For $R-I \approx 0.9$, approximately one in 10 of our stars have Hα in emission. With assumptions 2 and 3 above, this implies that typical dM2 stars have Hα in emission for approximately the first 10^9 years of their lifetimes. For $R-I \approx 1.2$, nearly one-third of the stars have Hα in emission, so the Hα emission period should be of the order of 3×10^9 years. A few of these stars may be relatively old and have Hα in emission only because they are members of short-period, binary systems; correction for this effect would slightly reduce our estimated time scales for the normal decay of Hα emission.

e) Hα *Absorption Widths and the Wilson-Bappu Effect*

The measured full width at half-maximum of the Hα absorption lines provides another means of comparing the new data with previous observations and theoretical predictions. Interest in the widths of chromospheric lines derives much of its impetus from the seminal paper by Wilson and Bappu (1957, hereafter WB) on the use of the Ca II K line reversal as a luminosity indicator. Later, Kraft, Preston, and Wolff (1964) showed that widths of the Hα absorption line could also be used for the same purpose for late-type stars. More recently, Zarro (1985) has discussed the use of Hα widths as a possible chromospheric diagnostic in M dwarfs.

We provide in Figure 11 a plot of our measured Gaussian sigmas versus $R-I$ (or M_V). Although there is considerable scatter, there is also a clear trend toward smaller widths for redder, fainter stars—which is the sense expected for the WB effect. A least-squares fit to the distribution yields $\sigma_{H\alpha} = -0.179(R-I)+0.447$, or, in terms of the FWHM (in angstroms), $H\alpha = -0.421(R-I)+1.05$. Using the main-sequence calibration from Stauffer *et al.* (1984), this corresponds to $M_V = 39.00-19.54\log H_\phi$, where H_ϕ is now measured in kilometers per second. The large slope and difficulty of obtaining highly accurate widths unfortunately makes the Hα width a poor luminosity indicator for M dwarfs; a 10% error in the width results in a 2 mag error in the luminosity.

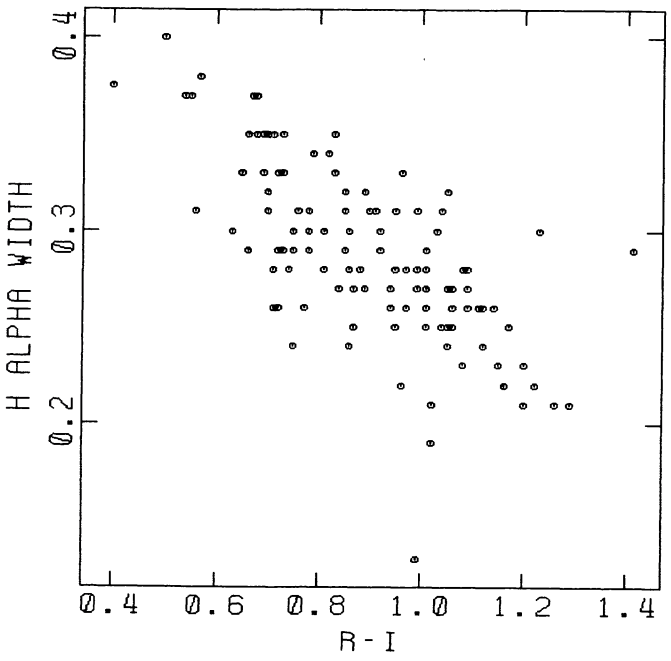

FIG. 11.—Gaussian width of the Hα absorption line versus $R-I$ for stars in Table 1.

IV. A SOLAR-METALLICITY MAIN-SEQUENCE RELATION FOR M DWARFS

There are a number of important problems which require knowledge of an accurate main-sequence relation for single, solar-metallicity, late-type dwarfs. Such a relation is a necessity in order to test the reliability of theoretical models of low-mass stars. For our own program, it is essential to have an accurate main-sequence calibration with which to compare our photometry of low-mass stars in young open clusters and thus derive luminosity differences between the observed pre–main-sequence loci and the standard main sequence. Distances to older open clusters from main-sequence fitting depend on an accurately known ZAMS.

A number of authors have previously attempted to derive main-sequence relations for M dwarfs, including Gliese (1969*b*), Upgren (1978), Dahn (1980), Mould and Hyland (1976), Veeder (1974*a*), Stauffer (1982*a*), and Stauffer *et al.* (1984). The Stauffer (1982*a*) relation was derived from a fit to the main sequences of the Hyades and Praesepe open clusters; the other calibrations are from field star data. Because $B-V$ is a poor temperature indicator for M dwarfs, in general these authors have used $R-I$ or $V-I$ as their temperature index. In Table 7 we provide a comparison of the various main-sequence calibrations, where we have formulated all of the relations to depend on $R-I$, using relations between $V-I$ and $R-I$ developed from our own photometry. A spread of several tenths of a magnitude exists among the various main-sequence relations, which is unacceptably large for many purposes. Part of the reason for this spread is that generally no corrections for binarity or metallicity have been applied to

TABLE 7

COMPARISON OF PREVIOUS MAIN-SEQUENCE (M_V, $R-I$)-RELATIONS[a]

$R-I$	V_{GL}	V_U	V_{TG}	V_{MH}	V_D	V_{S82}	V_{new}
0.60 ...	8.2	8.0	8.47	8.25	8.19	8.31	(8.43)
0.65 ...	8.4	8.3	8.77	8.55	8.47	8.61	8.69
0.70 ...	8.7	8.6	9.05	8.84	8.74	8.82	8.96
0.75 ...	9.0	8.9	9.33	9.14	9.01	9.07	9.22
0.90 ...	9.9	9.8	10.23	10.01	9.82	9.86	10.02
0.95 ...	10.2	10.1	10.54	10.37	10.09	10.11	10.28
1.00 ...	10.6	10.4	10.84	10.71	10.35	10.40	10.55
1.10 ...	11.2	11.0	11.50	11.39	10.89	11.03	11.08
1.20 ...	11.8	...	12.12	...	11.42	...	...

[a]The references for these calibration relations are Gliese 1969*b*, Upgren 1978, Tinsley and Gunn 1976, Mould and Hyland 1976, Dahn 1980, Stauffer 1982*a*, and this paper. The Tinsley and Gunn sequence is derived from Veeder's 1974*a* data; Veeder's own analysis concentrated on the (M_{BOL}, $V-K$)-plane.

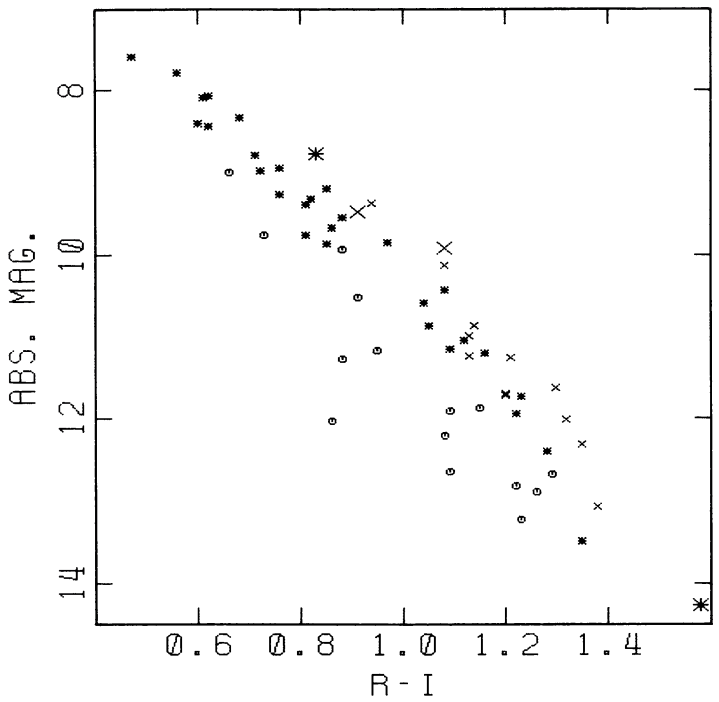

FIG. 12.—Color-magnitude diagram for the stars in Table 3. Open circles denote stars identified as subdwarfs by Mould and Hyland (1976), Upgren and Weis (1975), or Hartwick, Crampton, and Cowley (1976). Crosses indicate dMe stars. Double-sized symbols represent known binaries.

the photometry, simply because not enough information existed for the individual stars to make a systematic correction possible. With our new data base we hope to be able to make such corrections and thus derive a more reliable main-sequence calibration.

a) Gravity Indices and Infrared Colors for Subdwarfs

The stars for which we obtained low-dispersion spectra were originally observed in order to study a set of dM stars proposed to be subdwarfs by Upgren and Weis (1975), Mould and Hyland (1976), and Hartwick, Crampton, and Cowley (1976). A number of dMe stars were also observed. The Lick Observatory sample therefore serves as a good test case for examining the effects of age and metallicity on the position of M dwarfs in an H-R diagram. Figure 12 shows the (M_V, $R-I$)-diagram for the stars in Table 3. For a few stars without photometrically measured $R-I$ colors, we have used the $R-I$ estimates from the TiO band strengths listed in Table 3. Trigonometric parallaxes from van Altena (1985) have been used, as well as the parallax correction formulae proposed by Lutz and Kelker (1973). Only stars with $\sigma/\pi < 0.15$ are included in Figure 12. Stars shown as open circles were identified as subdwarfs by one or more of the above groups. The primary criterion for identification as a subdwarf by those authors was underluminosity in a color-magnitude diagram, so the displacement below the other stars in Figure 12 is neither surprising nor a new discovery.

It might be argued that the parallaxes or colors for these stars are significantly in error, and that some or all of them are not really subdwarfs. Observations of gravity-sensitive indices for a few of the subdwarf candidates by Mould and Hyland confirm high gravities for those stars. We will now provide similar evidence for the subdwarf candidates in Table 3. Plots of our gravity-sensitive indices versus $R-I$ are shown in Figure 13. The sense of all three indices indicates that higher gravity stars should have larger equivalent widths. Although there is a large amount of scatter in each diagram, which we attribute to the relatively low signal-to-noise ratio of most of our spectra, the proposed subdwarfs do appear to have higher gravities than the other stars. The three stars with the most consistently high gravities according to our indices, GL 15B, GL 543, and GL 699, also are the most subluminous stars in our sample.

We have established that the subdwarf candidates from Table 3 generally have high gravities as well as low luminosities. Following conventional wisdom, we presume that the underlying cause for these characteristics is that the subdwarfs are metal-poor. Mould and Hyland (1976) have proposed that both a ($B-V$, $R-I$)-diagram and a ($J-H$, $H-K$)-diagram are sensitive to metallicity variations for M dwarfs. Figures 14 and 15 show plots of these color sequences for the sample of stars provided in Table 3. Metal-poor stars should be red in $B-V$ for their $R-I$ and blue in $J-H$ for their $H-K$. The subdwarfs fall generally in the predicted region, which we take as confirmation that the two diagrams are indeed metal-sensitive.

b) A Main-Sequence Calibration Using Young dM Stars

We wish to determine the location in an (M_V, $R-I$)-plane for nonbinary, low-mass stars that have approximately solar metallicity, and that are old enough to have finished their pre–main-sequence evolution. Low-metallicity stars can be excluded by use of the ($J-H$, $H-K$)- and (Hα, $R-I$)-

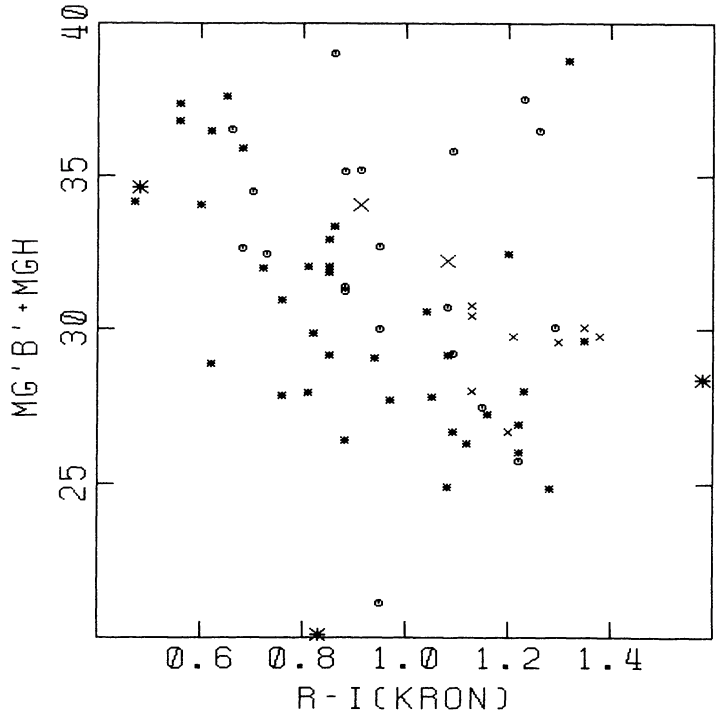

FIG. 13*a*

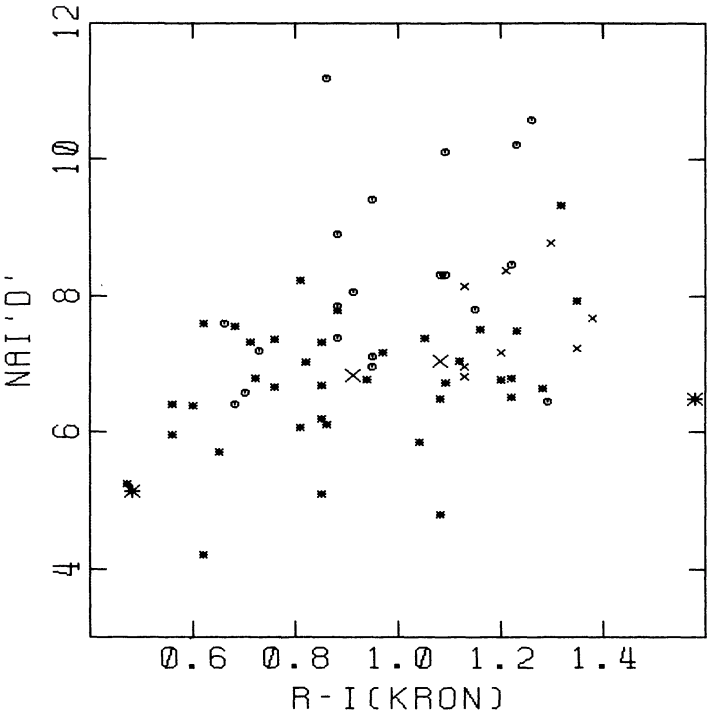

FIG. 13*b*

FIG. 13.—Panels *a*–*c* show the gravity indices for the M dwarfs observed at Lick plotted against $R - I$. Symbols are as in Fig. 12.

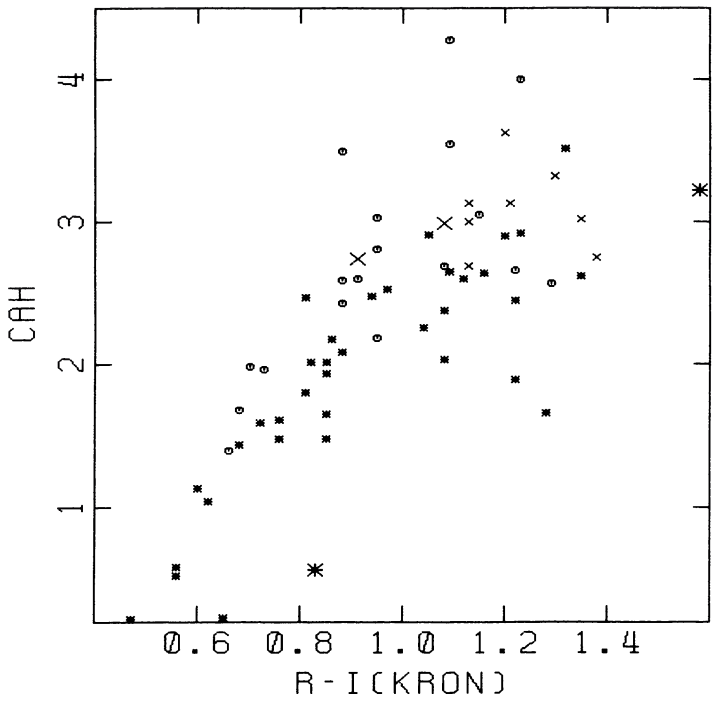

FIG. 13*c*

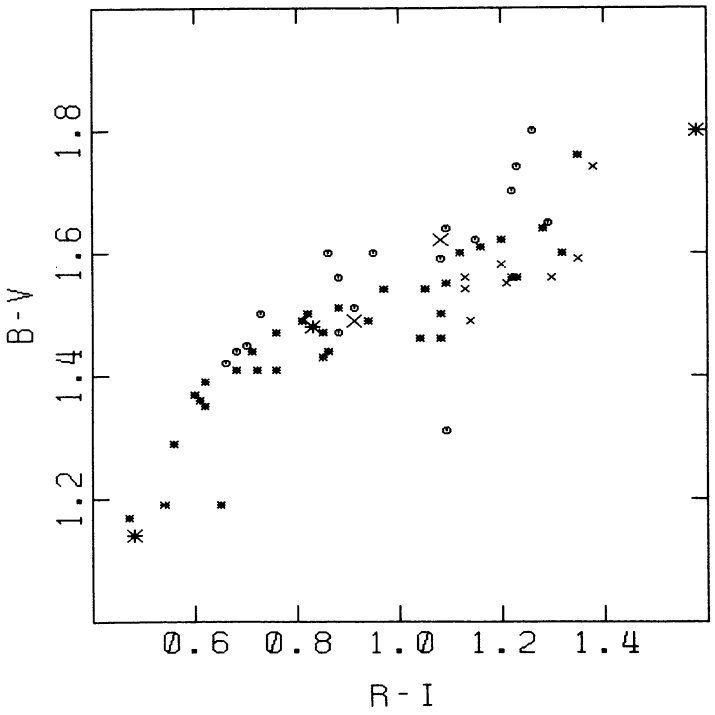

FIG. 14.—($B-V$, $R-I$)-diagram for stars in Table 3. Symbols are as in Fig. 13. Note that most of the subdwarf candidates are red in $B-V$ for their $R-I$ color.

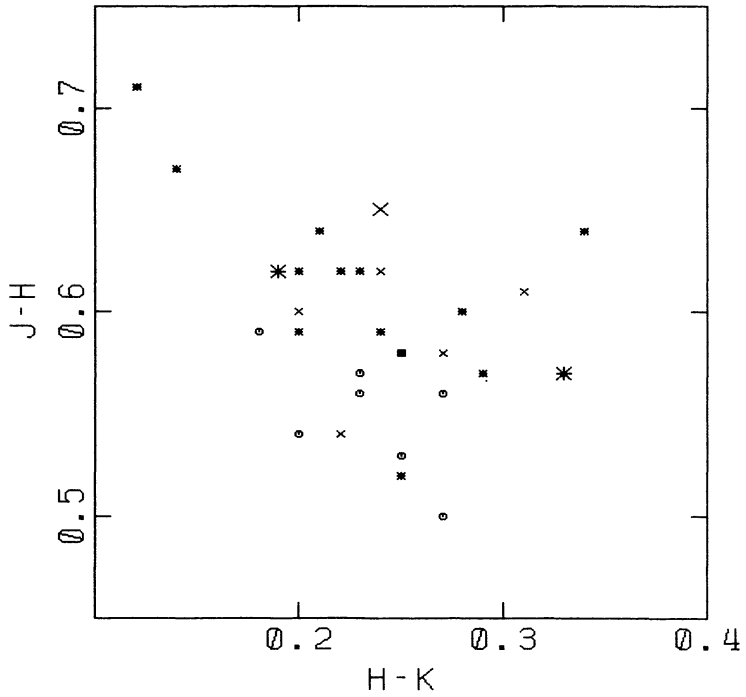

FIG. 15.—Infrared color-color diagram for stars in Table 3. The subdwarf candidates are generally blue in $J - H$ for their $H - K$ color.

diagrams. Very young M dwarfs can generally be avoided by excluding the dMe stars. We also exclude from consideration GL 98AB, GL 228AB, GL 643, and GL 747AB because of known or suspected binarity. The argument against GL 643 is that it is a spectroscopic binary according to Gliese (1969*a*), and it is generally considered a subdwarf (Joy 1947; Mould and McElroy 1978). Finally, stars with $\sigma/\pi > 0.15$ have also been culled because of the large Lutz-Kelker corrections that can be required. In Figure 16 we show the (M_V, $R - I$)-diagram for the entire sample given in Table 1 (Fig. 16*a*) and for just the presumed young and single subset selected here (Fig. 16*b*). It is clear that the selection process has succeeded in producing a much better defined main sequence, which should be more suitable for estimating the location of the solar-metallicity ZAMS.

Derivation of a solar-metallicity main-sequence locus from Figure 16*b* is still a subjective task, however. For an open cluster, the primary causes of the dispersion in such a diagram include (1) the presence of unresolved photometric binaries; (2) errors in the colors, resulting in magnitude errors of order $m\varepsilon$, where m is the slope of the main sequence and ε is the color error; and (3) differential distance moduli to the cluster members owing to the nonzero cluster radius. With reasonably good photometry and for clusters more distant than about 100 pc, the last two effects simply cause a small, calculable dispersion about the true main sequence. The binary stars can cause a displacement of up to about 1 mag relative to the true main sequence, but only in one direction. Therefore, the procedure for deriving a main-sequence locus is to fit a lower envelope to the cluster color-magnitude distribution, displaced upward by an amount corresponding to the dispersion induced by the color error and depth effect.

For our field star sample, binary stars and color errors are still present, and parallax errors take the place of the depth effect in the cluster. However, additional sources of error include the metallicity differences among the stars and the possibility that the youngest stars might still be contracting to the main sequence. We have, hopefully, eliminated the last problem by excluding the dMe stars from Figure 16*b*, and we have minimized but not eliminated the metallicity problem. For the moment we choose to assume that the metallicity range among the stars in Figure 16*b* is negligible. The displacement of the lower envelope fit should then be the sum in quadrature of the color-error term [$\Delta M_V = m\varepsilon(R - I) = 5 \times 0.015 = 0.075$ mag] and the parallax error. The average value of σ/π for the stars in Figure 16*a* is 0.073, corresponding to a 0.15 mag dispersion in M_V. The lower envelope fit should therefore be displaced upward by about 0.17 mag. Our "by-hand" fit to the lower envelope is shown in Figure 16*b* as the lower of the two lines. The upper curve represents the Hyades-Praesepe main-sequence relation adopted in Stauffer (1982*a*), as given in column (7) of Table 7. The new main-sequence relation is provided in column (8) of Table 7.

The fit to the lower envelope derived above should be a good estimate of the locus of the solar-metallicity main sequence if the stars in Figure 16*b* generally have solar metallicity or if the lower limit to the metallicity of these stars is approximately solar. There is, in fact, evidence for a metallicity spread even within our restricted sample. Mould (1978) has suggested that the upper envelope to the ($J - H$, $H - K$)

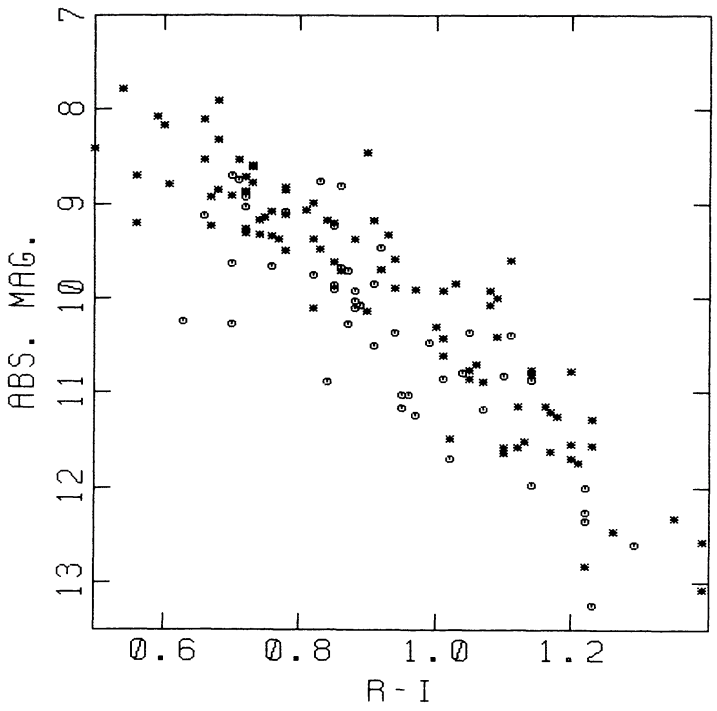

FIG. 16*a*

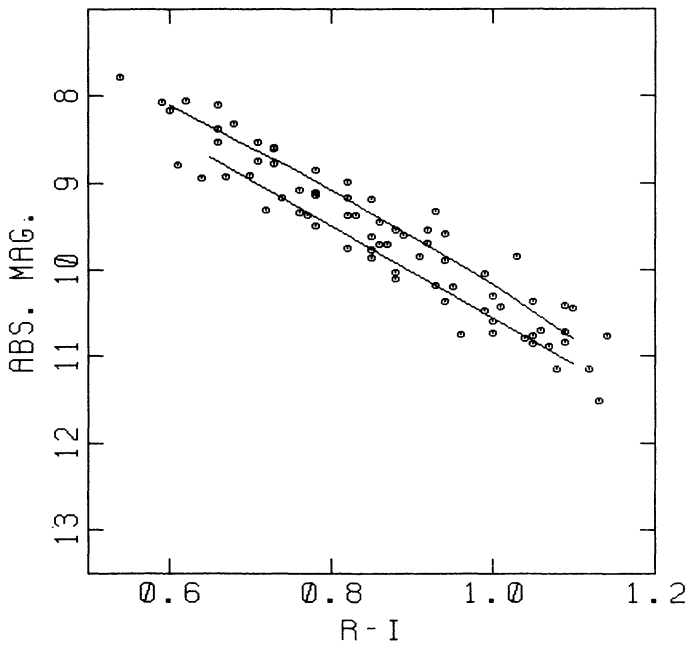

FIG. 16*b*

FIG. 16.—(*a*) Color-magnitude diagram for all stars in Table 1 for which appropriate photometry and parallax data are available. (*b*) The same diagram, but only for stars not known to be metal-poor, or binary, or with poorly determined parallaxes. The upper line is a main-sequence fit to stars in the Hyades and Praesepe open clusters, and the lower curve is the new proposed solar-metallicity main-sequence relation, as discussed in the text.

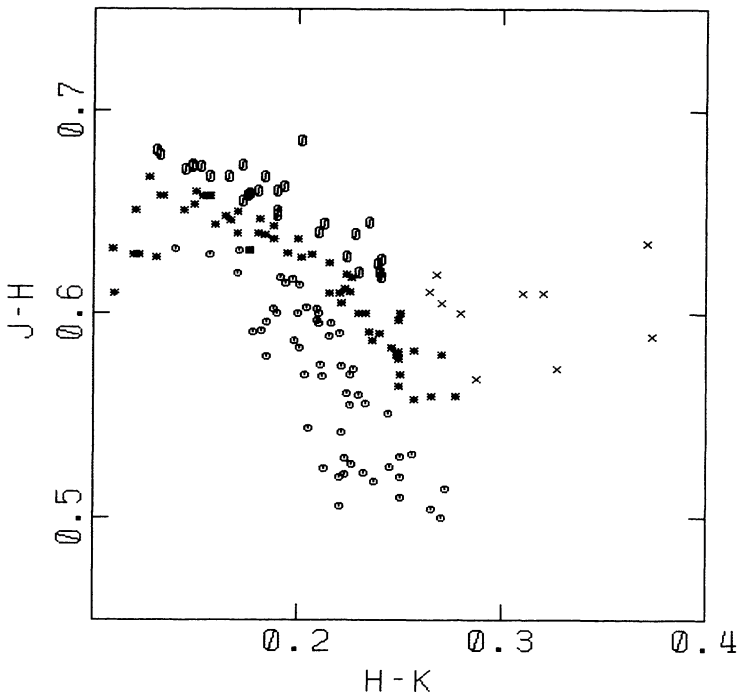

FIG. 17.—Infrared color-color diagram for the stars in Table 1. Stars denoted by oval symbols may have metallicities greater than solar according to Mould (1978). Crosses indicate very late type stars where no metallicity-color relation has been established.

distribution for M dwarfs harbors stars with metallicities greater than solar. Six of the stars in Mould and Hyland (1976) that defined an upper envelope in the infrared two-color diagram also roughly defined the bright limit for stars in their ($M_{\rm BOL}$, log T_e)-diagram. For one of these stars, GL 205, Fourier transform spectrometer (FTS) spectra allowed Mould to estimate [M/H] = +0.5.

To test Mould's hypothesis, we have identified a subset of our program stars that defines the upper envelope to our ($J-H$, $H-K$) distribution, as shown in Figure 17. Taking all of the stars from Figure 17 and plotting them in an (M_V, $R-I$)-diagram, we find that the metal-rich candidates have an average displacement above the main sequence of 0.50 mag, the "normal" metallicity sample has a mean displacement of 0.09 mag, and the metal-poor group is displaced below the main sequence by −0.20 mag. Excluding dMe stars or restricting the sample to stars with $\sigma/\pi < 0.15$ reduces the displacement of the metal-rich group to about 0.4 mag and does not change the results for the other group. This result appears to confirm Mould's prediction for these stars.

Based on Mould's estimated metallicity for GL 205, we infer that our $J-H$ bright stars have greater than solar metallicities. Fortunately, we have additional corroboration for this inference. Figure 18 shows an infrared two-color diagram for a set of Hyades M dwarfs. The Hyades photometry was obtained by us at KPNO during the same observing runs used to derive the field M dwarf data. The enclosed curve in Figure 18 defines the metal-rich region identified in Figure 17. It is apparent that the Hyades stars lie in the same region as the field, metal-rich candidates. This is appropriate, since the mean metallicity of Hyades members is generally believed to be about [M/H] = +0.15 (Chaffee, Carbon, and Strom 1971; Branch, Lambert, and Tomkin 1980). We note that the Hyades is much too old for stars in this mass range to be still contracting to the main sequence, hence there is no possible gravity interpretation of the location of the Hyades stars in the ($J-H$, $H-K$)-diagram.

Since the set of stars that we have now identified as more metal-rich than the Sun is included in Figure 16*b*, the upper envelope to the observed distribution of stars in that figure contains both binaries and metal-rich stars. In confirmation, the main-sequence relation derived from the fit to the Hyades and Praesepe (mean metallicity also generally taken to be [M/H] = +0.15) passes through the top portion of the field star distribution in Figure 16*b*. This is why we shaded our solar-metallicity fit toward the lower envelope to the distribution. If the supposed metal-rich stars do have [M/H] = +0.15 or more, then either Mould's empirical calibration of $\Delta M_{\rm BOL}/$[M/H] or the models of VandenBerg *et al.* (1983) predict a vertical displacement relative to solar-metallicity stars in the ($M_{\rm BOL}$, log T_e)-plane of about 0.25 mag. The observed displacement between the metal-rich and "normal" metallicity stars in our sample (excluding those with poorly determined parallaxes) is 0.3 mag in the (M_V, $R-I$)-plane. Assuming there are no strong blanketing corrections, the two estimates indicate that our main-sequence locus is not likely to be far off. In any case, it is unlikely that the true solar-metallicity main-sequence locus should be appreciably lower than we have placed it, and a locus much higher would conflict with the Hyades data.

V. THE NATURE AND ORIGIN OF dMe STARS

What specific characteristic of an M dwarf causes it to have Hα in emission? Certainly, one property that correlates well

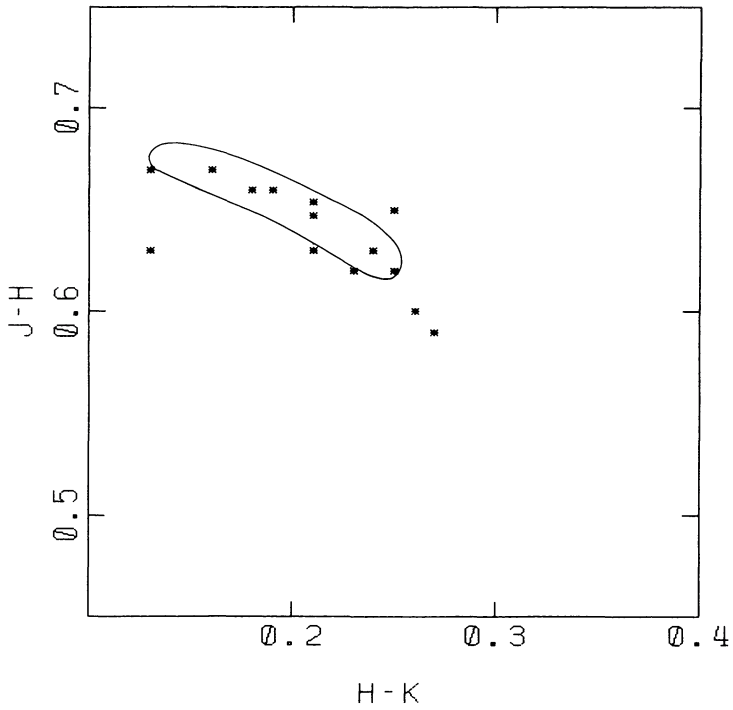

FIG. 18.—Hyades M dwarfs in the CIT system

with Balmer emission lines is youth. The space velocity diagrams shown in Figures 9 and 10, plus the fact that M dwarfs in young open clusters such as the Pleiades and α Persei clusters (Stauffer *et al.* 1984; Stauffer, Hartmann, and Jones 1985) have Hα in emission much more frequently than the field population, provide particularly strong evidence for this claim. However, there are some dMe stars, notably GL 781, GL 15B, and GL 812A, whose motions indicate that they are members of the old disk population. It has been suggested that rotation is the more fundamental parameter controlling chromospheric activity, with dMe stars being the most rapid rotators. Old stars could retain their emission-line properties if some process, such as tidal torque in a close binary orbit, had forced them to maintain a relatively high rotational velocity. There may also be other factors contributing to the origin of dMe stars. Joy (1947) and Veeder (1974*a*) have noted that dMe stars are on average more luminous than other M dwarfs of the same spectral type. This may indicate that many dMe stars are binaries, or that at least some of them are pre–main-sequence objects.

With the data gathered for this program, we have enough new, quantitative information to take a few small steps toward understanding dMe stars. We will first examine the rotational velocities and Hα profiles of our program stars, then consider how our photometric data can be used to constrain models for dMe stars, and finally compare the field dMe stars to M dwarfs in the Pleiades and Hyades. Previous papers of note on this subject are those of Veeder (1974*a*, hereafter V74), Veeder (1974*b*), Worden, Schneeberger, and Giampapa (1981, hereafter WSG), and Bopp and Espenak (1977).

a) *Rotational Velocities and* Hα *Profiles for dMe Stars*

The cross-correlation technique we have used to derive radial velocities also provides information on the width of the absorption lines in the spectra of our program stars. The resolution of the echelle spectrograph and the relatively low signal-to-noise ratio of our spectra set a lower limit on our line-broadening measurement at about 10 km s^{-1}. The possible broadening agents include microturbulence, macroturbulence, Zeeman broadening, the blending of lines from the two components of a binary system, and rotational broadening. With our resolution, we believe that the first three broadening mechanisms should not contribute to the cross-correlation peak width to a measurable degree. We note that Benz and Mayor (1984) ascribed an apparent excess width in the CORAVEL correlation peak widths for K and M dwarfs to Zeeman broadening. The excess broadening in the CORAVEL widths is only a few kilometers per second, however, too small to be detected with our spectra. With one or two possible exceptions, we do not find cross-correlation peak widths for any of our dM stars that are wider than the expected instrumental width. By contrast, many of the dMe stars do show detectable broadening of the cross-correlation peak.

In a number of cases, our spectroscopic data for specific dMe stars are inconclusive. More spectra are needed for each of these stars in order to determine their true rotational velocities and to decide whether peculiarities in their cross-correlation profiles are due to binarity, spottedness, or some other cause. The stars in this category are listed below.

GL 206.—Two spectra were obtained. One is clearly double peaked, with a velocity separation greater than 30 km s^{-1};

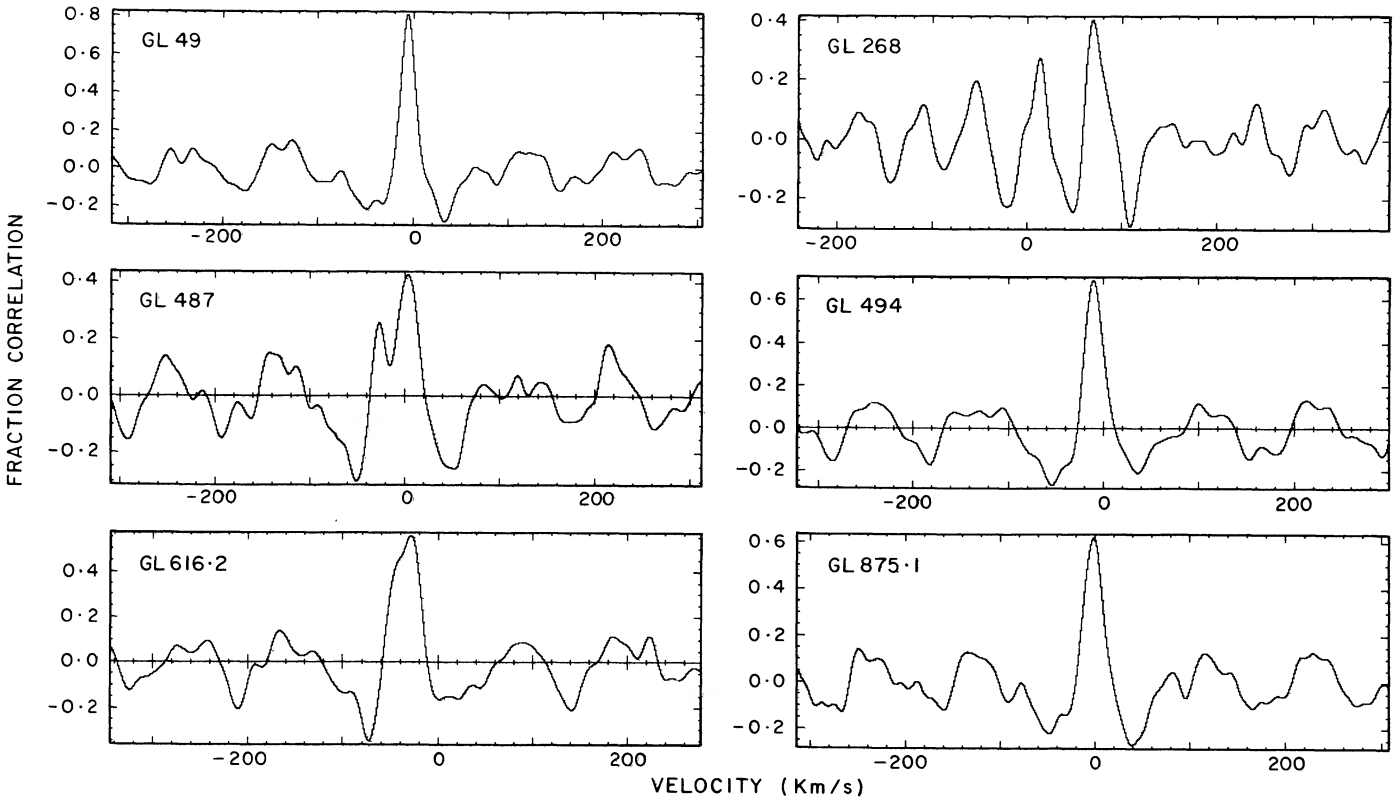

FIG. 19.—Cross-correlation profiles for a sample of M dwarfs. GL 49 is a dM star, and the width of its profile simply reflects our instrumental resolution (i.e., $v \sin i < 10$ km s^{-1}). With only one or two possible exceptions, all of our dM stars have equally sharp and symmetric cross-correlation profiles. The other five stars shown are dMe's. GL 268 is a large-amplitude SB2. The profiles for GL 494 and GL 875.1 are symmetric, but slightly broader than the instrumental profile.

the other spectrum is single peaked and essentially symmetric. The mean radial velocity is approximately the same for both spectra, however. This is probably an SB2.

GL 487.—Several spectra show quite asymmetric cross-correlation profiles, as illustrated in Figure 19. Presumably this is also an SB2.

GL 490B.—One spectrum shows an asymmetric cross-correlation profile. A possible SB2, but an appropriately spotted star could produce a similar profile (S. Vogt and D. Penrod 1985, private communication).

GL 616.2.—A large number of spectra of this star were obtained on two consecutive nights. On each night, the cross-correlation profile changed significantly on time scale of a few hours, going from nearly symmetric and only slightly broad to very asymmetric and moderately broad. A possible explanation is that this is a nearly pole-on, short-period binary.

GL 735.—One spectrum appears to show two well-separated cross-correlation profiles. A possible SB2.

GL 896B.—One spectrum shows an asymmetric cross-correlation profile. Either a spotted star or a binary.

In Table 8 we provide a summary of the cross-correlation results for the dMe stars; in Figure 19 we show representative examples of the cross-correlation profiles. We also list in Table 8 whatever other information is available on the rotational velocity and binarity of the program stars and the FWHM of the Hα profile, as well as a comment on the peak shape (centrally reversed, centrally peaked, asymmetric, and so on). The most obvious features of that table are the following:

1. Nearly half of the dMe stars have spectroscopic rotational velocities greater than 10 km s^{-1}. Our data are consistent with all of the dMe stars having rotational velocities greater than or equal to 5 km s^{-1}, the trigger velocity proposed for Hα emission by Bopp and Fekel (1977). Among the dMe stars, however, there is no obvious correlation between Hα equivalent width and $v \sin i$.

2. A significant fraction of the dMe stars are spectroscopic binaries. In two cases (GL 268 and GL 781) this may be connected with point 1, in that the claimed radial velocity range indicates orbital periods that are sufficiently short for tidal locking to have forced the rotational velocities of the components to be of order 5 km s^{-1}. The radial velocity variations for the other systems are small, suggesting that their orbital periods are long and that exchange of orbital angular momentum for rotation should have been insignificant. None of the dM stars appear as SB2's in our spectra.

3. There is a rough correlation between Hα emission profile and the star's rotational velocity. Stars with larger rotational velocities generally have centrally peaked Hα emission; the slower rotators have centrally reversed profiles. Significantly,

TABLE 8

ROTATION-ACTIVITY CONNECTION FOR dMe STARS

Star (GL) (1)	$J-H/H-K$ (2)	Space Motion (3)	Height above ZAMS (4)	$\Delta(B-V)$ (5)	$v \sin i$ (km s^{-1}) (6)	SB? (7)	Velocity Range (km s^{-1}) (8)	Hα (9)	FWHM (Å) (10)	Period (days) (11)
15B	MP	(OD)	0.97	0.15	...	...	...	...	...	...
82	...	YD	−0.52	−0.09	15	...	...	CP?	1.20	...
157B	...	...	...	...	<10	...	...	CR	1.13	...
206	MR	YD	−0.83	0.02	10	Y?	...	CP	1.29	...
207.1	...	YD	−0.52	0.01	10	...	...	CP	1.32	...
234A	MR	...	0.50	0.02	<10	...	...	CR	1.22	...
268	MR	OD	0.06	0.01	15	Y	110	D, CR	1.18	...
277A	MR	YD	−0.89	−0.09	<10	...	...	CR	1.29	...
277B	MR	YD	−0.49	−0.09	<10	...	...	CR	1.18	...
285	MR	YD	−0.09	−0.06	<10	...	...	CR?	1.15	2.8 P
362	MR	YD	−0.43	−0.05	<10	...	...	CR	1.20	...
388	...	YD	−0.25	−0.04	5	...	...	CR	1.18	2.6 P
487	MR	YD	+0.50	0.04	(10)	Y?	(15)	V	1.18	...
490A	...	OD	...	...	(8)	...	...	CR	1.18	3.2 P
490B	...	OD	...	...	>10	Y?	...	CP	1.53	...
494	MR	YD	−0.48	−0.01	10	...	...	CR	1.20	2.8 P
616.2	MR	OD	−0.82	0.01	?	Y?	(20)	CR/CP	1.29	...
644AB	MR	YD	+0.14	0.09	?	Y	40?	...	1.58	...
669A	MR	YD	−0.42	−0.06	<10	...	...	...	1.20	...
669B	...	...	+0.19	−0.08	<10	...	...	CR?	1.20	...
735	MR	YD	−1.03	−0.03	<10	Y?	...	CR	1.27	...
781	MP	OD	+1.30	0.11	15	Y?	(168)	CR?	1.25	...
812A	MP	(OD)	...	...	<10	...	...	CR	1.06	...
815AB.....	MP	OD	+0.59	+0.02	<10	Y	...	D, CR	1.20	3.2 O
831	...	...	...	...	<10	...	...	...	1.04	...
873	MR	YD	+0.09	−0.03	<10	...	...	CP?	1.32	...
875.1	MR	(OD)	−1.47	−0.06	11	...	...	CR	1.25	1.6 P
896A	...	YD	−0.01	−0.06	12	...	...	CP	1.39	...
896B	...	YD	...	...	18	...	...	CP	1.29	...

Col. (2)—MP = metal poor; MR = metal rich.

Col. (3)—OD = old disk; YD = young disk.

Col. (4)—Negative values indicate brighter than main-sequence relation. The magnitudes for GL 616.2 and GL 487 have been corrected to that for a single star assuming two equal mass members; GL 644AB and GL 815AB are assumed to be triple systems, with nearly equal mass components, and hence a magnitude correction of about 1.2 mag. See § II*c*.

Col. (5)—Negative indicates blue in $B-V$ for given $R-I$.

Col. (6)—Values in parentheses are particularly uncertain. The cross-correlation profiles for GL 487, GL 616.2, and GL 644AB are structured, indicating either that these stars are SB2, or that they are single but with large starspots causing unusual line profiles. It is uncertain, therefore, whether their broad cross-correlation profiles are due to the rotation of a single star or to the superposition of the spectra of two stars with slightly different radial velocities. Our preference is for the binary explanation.

Col. (7)—Y indicates the star is a known SB.

Col. (8)—Observed velocity range, from Gliese catalog or from this paper.

Col. (9)—CP = centrally peaked Hα emission, CR = centrally reversed, V = variable, D = double.

Col. (10)—FWHM of the Hα emission line, in angstroms.

Col. (11)—Rotational period of spotted star if followed by "P", orbital period if followed by "O."

all three metal-poor and presumably old dMe stars for which we have red echelle spectra have centrally reversed Hα emission. Worden, Schneeberger, and Giampapa (1981) noted a similar correlation between Hα emission profile and binarity; stars with centrally peaked Hα emission profiles generally belonged to short-period binaries.

There are still a number of dMe stars in our sample for which the present data only suggest $v \sin i < 10$ km s^{-1}. It is important to attempt to obtain better limits on rotational velocities for these stars in order to test the hypothesis of a trigger velocity for Hα emission. It would also be useful to obtain enough spectra to derive orbital parameters for the SB2 members of our sample.

The most important result of the echelle survey as it relates to the question of the origin of dMe stars is the strengthening of the correlation between rapid rotation and Hα emission. Our survey appears to be the first to have successfully detected rotational broadening for a significant number of dMe stars. Our success is due to the combination of the good sensitivity and high resolution of the MMT and 1.5 m echelle spectrographs, and the availability of a sophisticated software package to analyze the spectra.

b) Colors and Luminosities of dMe Stars

The photometric data for dMe stars also provide considerable insight into the nature of dMe stars. If dMe's are preferentially binaries, or if some of them are still contracting to the main sequence, they should lie above the single-star main-sequence locus. To test this prediction, Figure 20 reproduces the (M_V, $R-I$) data for our entire sample, with dMe stars shown as crosses. Known binary stars are denoted by double-sized symbols. The majority of the dMe stars do fall above the main-sequence curve, their mean displacement being 0.34 mag. A few notable exceptions to this rule exist, namely, GL 781 and GL 15B, which fall below the main sequence by 1.2 and 1.0 mag, respectively. The extremely high space velocity of GL 781 and its location in the metal-poor region of the ($J-H$, $H-K$)-diagram indicate that it is a subdwarf, halo(?) star. Interestingly, Gliese (1969*a*) lists GL 781 as an SB with a velocity range of 168 km s^{-1}. If this is true, our radial velocity from a single spectrum may be misleading. Two other dMe's, GL 812A and GL 815AB, have low metallicities according to the infrared color-color diagram. GL 815AB is a spectroscopic-visual triple system, of apparently three nearly equal mass stars (Fekel, Bopp, and Lacy 1978); if its absolute magnitude were corrected to that of a single star, it would lie significantly below the main sequence. GL 812A has an old disk space motion, but lies above the main sequence and is not known to have a secondary that could contribute significantly to the apparent luminosity.

Kuiper (1942) was the first to emphasize the overluminosity of the dMe stars. Veeder (V74) concurred, but he also noted exceptions to the rule. Veeder considered binarity and pre–main-sequence evolution as possible explanations for the overluminosity, but rejected both. Binarity as an explanation for the dMe's makes sense only if the systems have short enough period for orbital-rotational angular-momentum exchange, and a number of the overluminous dMe stars have good enough spectral coverage to indicate that they are single or at least have no companion close enough and massive enough to be important. The pre–main-sequence explanation requires very young ages for the dMe's, which is incompatible with the old disk motions exhibited by some of them. Also, if they are young enough to be significantly above the main sequence, some of them should have $v \sin i > 40$ km s^{-1}, as do nine of the 20 Pleiades M dwarfs with measured spectroscopic rotational velocities (Stauffer *et al.* 1984; Stauffer and Hartmann 1985). Some dMe stars could be overluminous as a result of binarity or PMS evolution, but it is unlikely that these are the dominant processes causing the overluminosity. A third possibility that Veeder considered was high metallicity. This was the explanation favored by Veeder, because it seemed to conflict least with existing data. In this model, the photometric properties of dMe stars are directly explained by their metallicities, whereas the chromospheric activity is only indirectly connected through an assumed metallicity-age-rotation correlation.

If most dMe stars are metal-rich, they should have peculiar locations in color-color diagrams. Our data confirm that prediction. Excluding the 10 very late type stars shown as crosses (six of which are dMe stars, simply because most very late type stars have Hα in emission), there are 151 stars plotted in

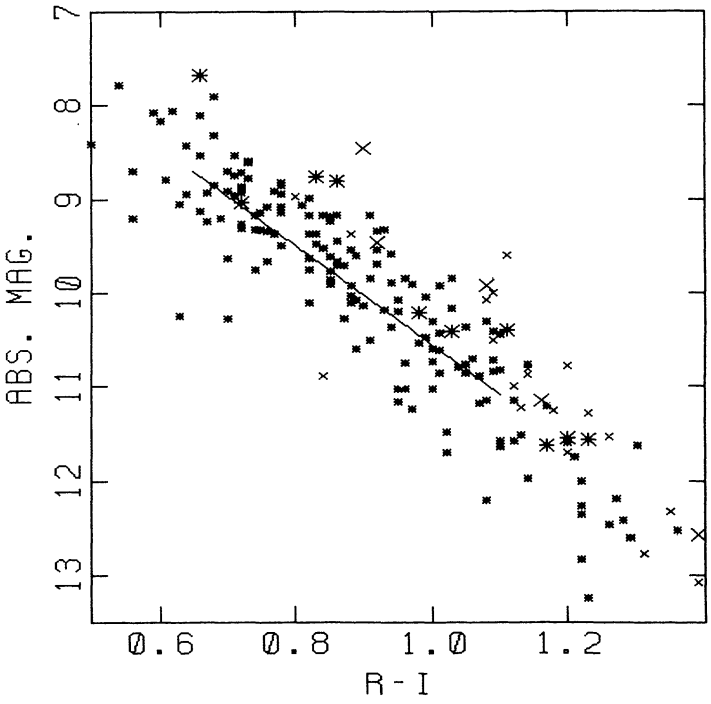

FIG. 20.—Color-magnitude diagram for stars in Table 1. Stars known to be binary are marked as double-sized symbols; dMe stars are shown as crosses.

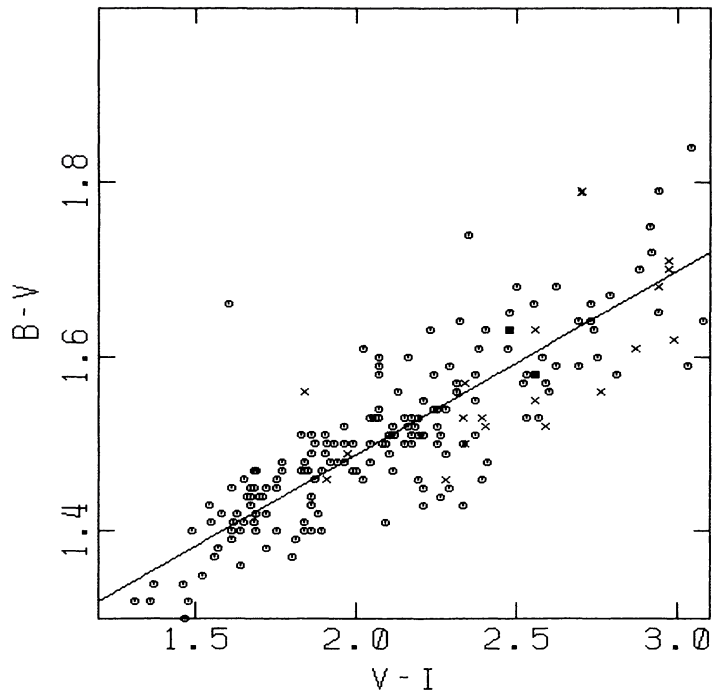

FIG. 21.—Correlation between $B-V$ and $V-I$ for the stars from Table 1. Symbols are as in Fig. 20. Note that dMe stars are generally blue in $B-V$ for their $V-I$. The most obvious exceptions to this rule are GL 15B ($B-V=1.79$, $V-I=2.27$) and GL 781 ($B-V=1.56$, $V-I=1.84$).

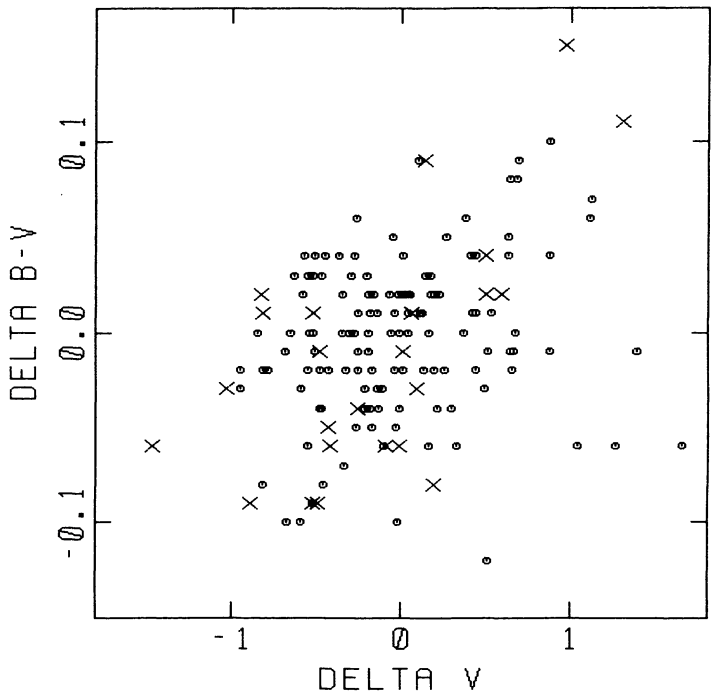

FIG. 22.—The difference between the observed $B-V$ for a given star and the fit to the ($B-V$, $V-I$) distribution shown in Fig. 21 plotted against the displacement relative to the main sequence shown in Fig. 20. Absolute magnitudes for the stars known to be binaries of approximately equal mass have been corrected to that for a single star.

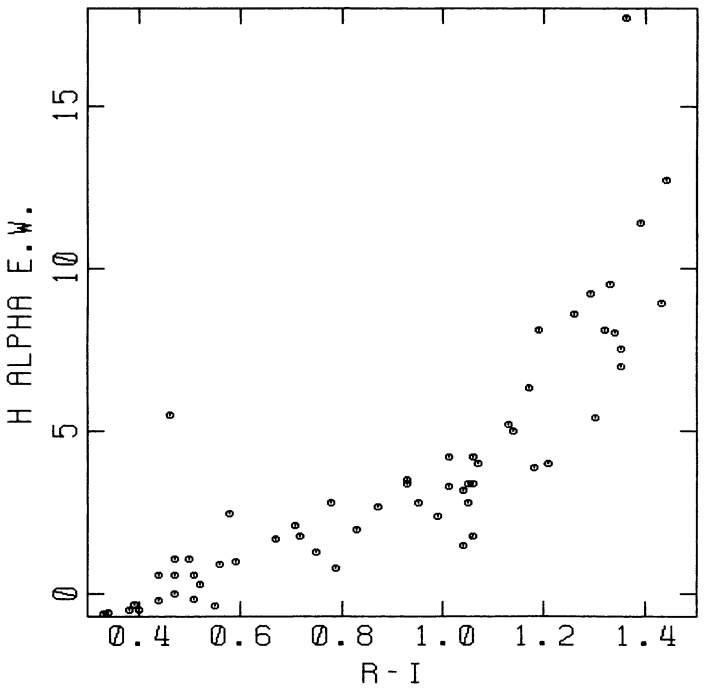

FIG. 23*a*

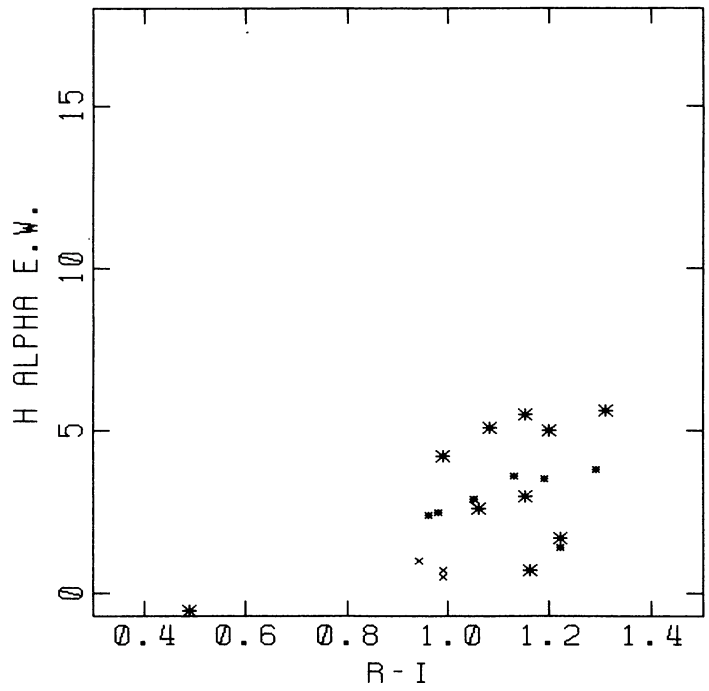

FIG. 23*b*

FIG. 23.—Correlation between Hα equivalent width and $R-I$ color for M dwarfs in (*a*) the Pleiades and (*b*) the Hyades. For the Hyades panel, small symbols indicate low-quality observations. Crosses indicate upper limits.

Figure 17. Eighteen of those 151 stars (or 12%) are dMe's. Yet among the 32 stars identified as possibly metal-rich because of their red $J-H$ colors, nine (28%) are emission-line stars. Seven of the 12 weak Hα, active chromosphere candidates from Table 5 are also in the metal-rich regions of the ($J-H$, $H-K$)-diagram. Further evidence arises from consideration of the $B-V$ colors of the dMe stars. To illustrate this point, we have fitted a straight line through the ($B-V$, $V-I$) distribution of the stars in our sample, as shown in Figure 21 ($R-I$ or $V-K$ could have been used as the red color, but $V-I$ seemed the best choice for providing a large sample and showing relatively small scatter). We have then calculated deviations from that relation as a function of $V-I$. Those deviations, $\Delta(B-V)$, are plotted against the vertical displacement of a star from the (M_V, $R-I$) calibration in Figure 22. This diagram shows that the dMe stars that are displaced above the main sequence are generally blue in $B-V$ for their $V-I$ color. By contrast, the few dMe stars that fall below the main sequence are relatively red in $B-V$. This is precisely the effect predicted by metallicity differences.

c) *Comparison with the Pleiades and Hyades M Dwarfs*

One set of M dwarfs with which we can compare our field sample have both known ages and known metallicities. Those stars are the dMe members of the Pleiades and Hyades, which we have observed concurrently with the field sample. We have already used some of the photometric data for the Hyades in the preceding discussions. The Pleiades dM stars are faint, and the accuracy of our $B-V$ and $J-H$ photometry for the Pleiades sample is too poor to add much to the present discussion. We do, however, have a large body of Hα equivalent widths which are sufficiently accurate to be of use. Figure 23 shows the (Hα, $R-I$) correlation for the two clusters. A few of the Hyades points are derived from 7 Å resolution IDS spectra, and are thus of low weight; the remaining points are from MMT echelle spectra, and should be of similar accuracy to the field sample. The comparison with the field data is very interesting. All of the Pleiades M dwarfs have Hα in emission, with the equivalent width increasing monotonically to later type stars. The Hyades stars may also all have Hα in emission; the few points shown as upper limits were derived from either low-resolution or low signal-to-noise spectra. The upper envelope to the field dMe (Hα, $R-I$) distribution falls on or slightly below the Pleiades sample, and is generally consistent with the Hyades stars. This probably indicates that the youngest field dMe stars in our sample have ages of the order of a few times 10^8 years.

Our spectroscopic rotational velocities also indicate an age closer to the Hyades stars for the field dMe's. Nearly one-half of the Pleiades dM stars have $v \sin i > 40$ km s^{-1}. Echelle spectra for a large number of Hyades dM stars have been obtained (Latham 1985) but not yet analyzed for rotational velocity. However, visual inspection of the cross-correlation profiles indicates that at most a few, and possibly none, have $v \sin i > 30$. Our field dMe sample also contains no stars with large $v \sin i$, though some of the dMe stars show detectable rotation whereas none of the dM stars do, indicating a characteristic age similar to or older than the Hyades.

VI. SUMMARY AND DESIDERATA

By a combination of observational techniques, we have sorted our M dwarf sample into a number of subsets ordered by metallicity and chromospheric activity. We have identified a few new dMe stars, plus a few stars that were previously dMe and now appear to be less active. A number of other stars have chromospheres just slightly less active than the dMe's, and may prove to be good targets for future observations. We have used the photometric information for our dM sample to select a set of single stars to define a solar-metallicity main sequence. A fit to the Hyades lower main sequence (distance modulus = 3.30) is displaced about 0.3 mag above the new field star main sequence, in approximate accord with the expected displacement if the Hyades metallicity is [M/H] $= +0.15$. The unusual photometric properties of dMe stars appear to be controlled by their metallicities, while their chromospheric activity is most closely linked with their rotational velocities.

We believe that a number of approaches would prove fruitful in continuing to refine our knowledge of low-mass stars. We particularly suggest the following: (1) the apparently old, dMe stars GL 15B, GL 781, and GL 812A should be monitored for the radial velocity variability predicted in § V; (2) broad-band differential photometry and/or high signal-to-noise spectra at Hα or Ca II K should be obtained to search for spot modulation in the sample of stars that may have composite chromospheres; (3) FTS spectra, or some other method yielding quantitative metallicities, should be obtained for stars with accurate infrared photometry in order to calibrate the ($J-H$, $H-K$)-diagram for metallicity; and (4) a larger sample of Hyades M dwarfs should be surveyed at higher signal-to-noise to better define the (Hα, $R-I$)-relation for Hyades age stars.

We wish to thank Ed Horine and Jim Peters for obtaining many of the echelle spectra used for this study. Peter Stetson provided the software package from which most of the plots in this paper were produced. We thank A. Dupree for allowing us to examine her spectra of GL 616.2, and W. van Altena for allowing us to use a prepublication copy of the new parallax catalog. The software routines for analyzing the echelle spectra were written by John Tonry, Neal Burnham, and Rob Hewett. We thank S. Vogt and D. Penrod for useful discussions.

REFERENCES

Benz, W., and Mayor, M. 1984, *Astr. Ap.*, **138**, 183.
Bopp, B., Africano, J. L., Stencel, R. E., Noah, P. V., and Klimke, A. 1983, *Ap. J.*, **275**, 691.
Bopp, B., and Espenak, F. 1977, *A.J.*, **82**, 916.
Bopp, B., and Fekel, F. 1977, *A.J.*, **82**, 490.
Branch, D., Lambert, D. L., and Tomkin, J. 1980, *Ap. J.* (*Letters*), **241**, L83.
Chaffee, F. G., Carbon, D. F., and Strom, S. E. 1971, *Ap. J.*, **166**, 593.
Chugainov, P. F. 1974, *Izv. Krymsk. Ap. Obs.*, **52**, 3.
Cram, L. E., and Mullan, D. J. 1979, *Ap. J.*, **234**, 579 (CM).

Dahn, C. 1980, private communication.
Deeming, T. J. 1960, *M.N.R.A.S.*, **121**, 52.
Duncan, D., Baliunas, S. L., Noyes, R. W., Vaughan, A. H., Frazer, J., and Lanning, H. 1984, *Pub. A.S.P.*, **96**, 707.
Durney, B. R., Mihalas, D., and Robinson, R. 1981, *Pub. A.S.P.*, **93**, 537.
Eggen, O. J. 1971, *Ap. J. Suppl.*, **22**, 389.
_____. 1975, *Pub. A.S.P.*, **87**, 107.
_____. 1979, *Ap. J. Suppl.*, **39**, 89.
_____. 1980, *Ap. J. Suppl.*, **43**, 457.
Elias, J. H., Frogel, J. A., Matthews, K., and Neugebauer, G. 1982, *A.J.*, **87**, 1029.
Fekel, F., Bopp, B. W., and Lacy, C. H. 1978, *A.J.*, **83**, 1445.
Fosbury, R. A. 1974, *M.N.R.A.S.*, **169**, 147.
Frogel, J. A., Persson, S. E., Aaronson, M., and Matthews, K. 1978, *Ap. J.*, **220**, 75.
Giampapa, M. S. 1985, *Ap. J.*, **299**, 781.
Glass, I. S. 1974, *M.N.A.S. So. Africa*, **33**, 53.
Gliese, W. 1969*a*, *Veröff. Astr. Rechen-Inst. Heidelberg*, No. 22.
_____. 1969*b*, in *Low-Luminosity Stars*, ed. S. S. Kumar (New York: Gordon & Breach), p. 41.
Goad, J. 1982, Kitt Peak National Observatory Facilities Manual.
Harrington, R. S., and Dahn, C. C. 1980, *A.J.*, **85**, 454.
Hartwick, F. D. A. 1977, *Ap. J.*, **234**, 778.
Hartwick, F. D. A., Crampton, D., and Cowley, A. P. 1976, *Ap. J.*, **208**, 776.
Herbig, G. 1985, *Ap. J.*, **289**, 269.
Joy, A. H. 1947, *Ap. J.*, **105**, 96.
Joy, A. H., and Abt, H. A. 1974, *Ap. J. Suppl.*, **28**, 1.
Kraft, R. H., Preston, G. W., and Wolff, S. C. 1964, *Ap. J.*, **140**, 237.
Kron, G. 1950, *A.J.*, **55**, 69.
Kron, G., Gascoigne, S., and White, H. 1957, *A.J.*, **62**, 205 (KGW).
Krzeminski, W. 1969, *Low-Luminosity Stars*, ed. S. Kumar (New York: Gordon & Breach), p. 57.
Kuiper, G. P. 1942, *Ap. J.*, **95**, 201.
Landolt, A. 1983, *A.J.*, **88**, 439.
Latham, D. 1985, in *IAU Colloquium 88*, *Stellar Radial Velocities*, ed. A. G. D. Philip and D. W. Latham (Schenectady: Davis), p. 21.
Linsky, J. L., and Ayres, T. R. 1978, *Ap. J.*, **220**, 619.
Lutz, T. E., and Kelker, H. 1973, *Pub. A.S.P.*, **85**, 573.
Miller, J., Robinson, L., and Wampler, E. J. 1976, in *Adv. Electronics Electron Phys.* (New York: Academic), p. 693.
Moffett, T., and Barnes, T. 1979, *A.J.*, **84**, 627.
Mould, J. R. 1976*a*, *Astr. Ap.*, **48**, 443.
_____. 1976*b*, *Ap. J.*, **207**, 535.
_____. 1978, *Ap. J.*, **226**, 923.
_____. 1985, private communication.
Mould, J. R., and Hyland, A. R. 1976, *Ap. J.*, **208**, 399.
Mould, J. R., and McElroy, D. B. 1978, *Ap. J.*, **220**, 935.
Mundt, R., Walter, F., Feigelson, E., Finkenzeller, U., Herbig, G., and Odell, A. 1983, *Ap. J.*, **269**, 229.
Noyes, R. W., Hartmann, L., Baliunas, S. L., Duncan, D. K., and Vaughan, A. H. 1984, *Ap. J.*, **279**, 763.
Ohman, Y. 1934, *Ap. J.*, **80**, 171.
Oke, J. B. 1974, *Ap. J. Suppl.*, **27**, 21.
Parker, E. N. 1979, *Cosmical Magnetic Fields: Their Origin and Activity* (Oxford: Clarendon Press).
Persson, S. E., Aaronson, M., and Frogel, J. A. 1977, *A.J.*, **82**, 729 (PAF).
Petit, J. 1961, *J. d. Obs.*, **44**, 11.
Pettersen, B. R., Evans, D. S., and Coleman, L. A. 1984, *Ap. J.*, **282**, 214.
Simon, T., Herbig, G., and Boesgaard, A. M. 1985, *Ap. J.*, **293**, 551.
Spinrad, H. 1973, *Ap. J.*, **183**, 923.
Stauffer, J. 1980, *A.J.*, **85**, 1341.
_____. 1982*a*, *A.J.*, **87**, 899.
_____. 1982*b*, *A.J.*, **87**, 1507.
_____. 1984, *Ap. J.*, **280**, 189.
Stauffer, J., and Hartmann, L. 1985, in *Proc. Fourth Cambridge Workshop on Cool Stars, Stellar Systems and the Sun*, ed. M. Zeilik (Berlin: Springer).
Stauffer, J., Hartmann, L., and Jones, B. F. 1985, *Ap. J.*, **289**, 247.
Stauffer, J., Hartmann, L., Soderblom, D. R., and Burnham, J. N. 1984, *Ap. J.*, **280**, 202.
Stone, R. P. S. 1977, *Ap. J.*, **218**, 767.
Tinsley, B., and Gunn, J. R. 1976, *Ap. J.*, **203**, 52.
Tonry, J., and Davis, M. 1979, *A.J.*, **84**, 1511.
Upgren, A. R. 1978, in *IAU Symposium 80*, *The HR Diagram*, ed. A. G. D. Philip and D. S. Hayes (Dordrecht: Reidel), p. 39.
Upgren, A. R., and Weis, E. W. 1975, *Ap. J.* (*Letters*), **197**, L53.
van Altena, W. F. 1985, private communication.
VandenBerg, D. A., Hartwick, F. D. A., Dawson, P., and Alexander, D. R. 1983, *Ap. J.*, **266**, 747.
Vaughan, A. H., Baliunas, S. L., Middlekoop, F., Hartmann, L., Mihalas, D., Noyes, R. W., and Preston, G. W. 1981, *Ap. J.*, **250**, 276.
Vaughan, A. H., and Preston, G. W. 1980, *Pub. A.S.P.*, **92**, 385.
Veeder, G. J. 1974*a*, *A.J.*, **79**, 1056 (V74).
_____. 1974*b*, *A.J.*, **79**, 702.
Vernazza, J. E., Avrett, E. H., and Loeser, R. 1981, *Ap. J. Suppl.*, **45**, 635.
Weis, E. W. 1982, *A.J.*, **87**, 152.
Weis, E. W., and Upgren, A. R. 1982, *Pub. A.S.P.*, **94**, 821.
Wilson, O. C. 1966, *Ap. J.*, **144**, 695.
_____. 1967, *A.J.*, **72**, 905.
_____. 1978, *Ap. J.*, **226**, 379.
Wilson, O. C., and Bappu, M. K. V. 1957, *Ap. J.*, **125**, 661 (WB).
Woolley, R., Epps, E. A., Penston, M. J., and Pocock, S. B. 1970, *A Catalogue of Stars within 25 Parsecs of the Sun* (*Roy. Obs. Ann.*, No. 5).
Worden, S. P., Schneeberger, T. J., and Giampapa, M. S. 1981, *Ap. J. Suppl.*, **46**, 159 (WSG).
Young, A., Skumanich, A., and Harlan, E. 1984, *Ap. J.*, **282**, 683.
Young, A., Skumanich, A., Stauffer, J., Hartmann, L., and Bopp, B. 1986, in preparation (Paper I).
Zarro, D. M. 1983, *Ap. J.* (*Letters*), **267**, L61.
_____. 1985, *Ap. J.*, **291**, 297.
Zarro, D. M., and Rodgers, A. W. 1983, *Ap. J. Suppl.*, **53**, 815.

LEE W. HARTMANN: Harvard-Smithsonian Center for Astrophysics, 60 Garden Street, Cambridge MA 02138

JOHN R. STAUFFER: Dominion Astrophysical Observatory, 5071 W. Saanich Road, Victoria, BC, V8X 4M6, Canada